HHS Public Access

Author manuscript

Cell. Author manuscript; available in PMC 2019 March 22.

Published in final edited form as:

Cell. 2018 March 22; 173(1): 117–129.e14. doi:10.1016/j.cell.2018.03.001.

Amino acid restriction triggers angiogenesis via GCN2/ATF4 regulation of VEGF and H_2S production

Alban Longchamp[1,2,**], **Teodelinda Mirabella**[3,4,**], **Alessandro Arduini**[1,**], **Michael R. MacArthur**[1], **Abhirup Das**[5,6], **J. Humberto Treviño-Villarreal**[1], **Christopher Hine**[1], **Issam Ben-Sahra**[1], **Nelson H. Knudsen**[1], **Lear E. Brace**[1], **Justin Reynolds**[1], **Pedro Mejia**[1], **Ming Tao**[2], **Gaurav Sharma**[2], **Rui Wang**[7], **Jean-Marc Corpataux**[8], **Jacques-Antoine Haefliger**[8], **Kyo Han Ahn**[9], **Chih-Hao Lee**[1], **Brendan D. Manning**[1], **David A. Sinclair**[5,6], **Christopher S. Chen**[3,4], **C. Keith Ozaki**[2], and **James R. Mitchell**[1,*]

[1]Dept of Genetics and Complex Diseases, Harvard T. H. Chan School of Public Health, Boston, MA 02115, USA [2]Dept of Surgery and the Heart and Vascular Center, Brigham & Women's Hospital and Harvard Medical School, Boston, MA 02115, USA [3]Tissue Microfabrication Lab, Dept of Biomedical Engineering Boston University, Boston, MA 02115, USA [4]Wyss Institute for Biologically Inspired Engineering, Boston, MA 02115, USA [5]Glenn Center for the Biological Mechanisms of Aging, Dept of Genetics, Harvard Medical School, Boston, MA 02115, USA [6]Laboratory for Ageing Research, Dept of Pharmacology, School of Medical Sciences, The University of New South Wales, Sydney NSW 2052, Australia [7]Cardiovascular and Metabolic Research Unit, Laurentian University, Sudbury, ON, Canada [8]Dept of Vascular Surgery, Laboratory of Experimental Medicine, Centre Hospitalier Universitaire Vaudois, Lausanne, Switzerland [9]Dept of Chemistry, Postech, 77 Cheongam-Ro, Nam-Gu, Pohang, 37673, Republic of Korea

Summary

Angiogenesis, the formation of new blood vessels by endothelial cells (EC), is an adaptive response to oxygen/nutrient deprivation orchestrated by vascular endothelial growth factor (VEGF) upon ischemia or exercise. Hypoxia is the best-understood trigger of VEGF expression via the transcription factor HIF1α. Nutrient deprivation is inseparable from hypoxia during ischemia, yet its role in angiogenesis is poorly characterized. Here, we identified sulfur amino acid restriction as a proangiogenic trigger, promoting increased VEGF expression, migration and

*Lead contact: jmitchel@hsph.harvard.edu.
**equal contribution

Declaration of Interests

The authors declare no competing interests.

Author Contributions

Conceptualization: A.L., T.M., A.A., M.R.M., A.D., C.H., C.S.C., C.K.O., J.R.M.; Methodology: A.L., T.M., A.A., M.R.M., J.H.T.-V., C.H., I.B.-S., N.H.K., L.E.B.; Investigation: A.L., T.M., A.A., M.R.M., A.D., J.H.T.-V., C.H., I.B.-S., N.H.K., L.E.B., J.R., P.M., M.T., G.S; Resources: R.W., J.- M.C., J-A.H., K.H.A, C.-H.L., B.D.M., D.A.S., C.S.C., C.K.O., J.R.M.; Writing, A.L., J.R.M.; Funding Acquisition, A.L., C.K.O., J.R.M.

sprouting in EC *in vitro,* and increased capillary density in mouse skeletal muscle *in vivo,* via the GCN2/ATF4 amino acid starvation response pathway independent of hypoxia or HIF1α. We also identified a requirement for cystathionine-γ-lyase in VEGF-dependent angiogenesis via increased hydrogen sulfide (H_2S) production. H_2S mediated its proangiogenic effects in part by inhibiting mitochondrial electron transport and oxidative phosphorylation, resulting in increased glucose uptake and glycolytic ATP production.

Graphical Abstract

Restricting dietary sulfur can trigger angiogenesis and improve vascular health

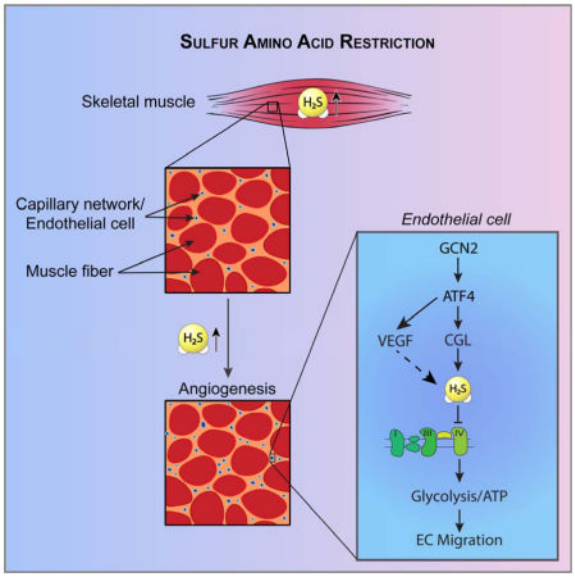

Introduction

Angiogenesis is the formation of new blood vessels from existing ones through sprouting, proliferation and migration of endothelial cells (EC). In adult mammals, angiogenesis is an adaptive response to normal and pathophysiological conditions characterized by inadequate supply of oxygen and nutrients, ranging from tissue ischemia upon vessel occlusion or tumorigenesis to endurance exercise.

Hypoxia is the best-understood trigger of angiogenesis, stabilizing the oxygen-sensitive transcription factor hypoxia inducible factor (HIF)-1α in multiple cell types and promoting expression of the master regulator of angiogenesis, vascular endothelial growth factor (VEGF). VEGF expression can also be induced by the transcriptional co-activator PGC1α upon nutrient deprivation through an ERR-α-dependent, HIF-1α independent pathway in muscle cells but not EC (Arany et al., 2008), as well as by the ATF4 transcription factor downstream of the integrated stress response (ISR) triggered by either ER stress or amino acid (AA) deprivation (Abcouwer et al., 2002).

VEGF acts via binding to EC-specific cell-surface tyrosine kinase receptors (VEGFR2), triggering an orchestrated cascade of signal transduction via the PI3K and MAPK pathways

involving critical second messengers nitric oxide (NO) and cyclic GMP (cGMP) and changes in gene expression facilitating EC migration, proliferation and vessel formation (Olsson et al., 2006). VEGF-mediated angiogenesis is potentiated by the NAD+-dependent deacetylase SIRT1, which deacetylates and inactivates FOXO transcription factors (Potente et al., 2007) involved in negative regulation of EC migration and tube formation (Potente et al., 2005). VEGF signalling also triggers changes in cellular energy metabolism, namely increased glucose uptake and glycolysis necessary to provide rapid energy for EC migration (De Bock et al., 2013).

Hydrogen sulfide (H_2S) is a proangiogenic gas (Cai et al., 2007; Szabo, 2007) produced in EC upon VEGF stimulation (Papapetropoulos et al., 2009) primarily by the transsulfuration enzyme cystathionine-γ-lyase (CGL aka CTH or CSE) (Wang, 2012). Like NO, which in addition to activating cGMP synthesis functions through post-translational modification (S-nitrosylation) of target proteins (Fukumura et al., 2006), H_2S promotes angiogenesis through S-sulfhydration and activation of proximal signal transduction components including VEGFR2 (Tao et al., 2013) and eNOS (Altaany et al., 2014; Coletta et al., 2012). Angiogenesis is compromised upon genetic CGL deficiency in aorta explant assays *ex vivo* (Papapetropoulos et al., 2009) and arterial ligation *in vivo* (Kolluru et al., 2015). However, mechanisms of CGL regulation in EC and the relative contribution of H_2S vs. NO in angiogenesis remain unclear (Katsouda et al., 2016).

Dietary restriction (DR), defined as reduced nutrient/energy intake without malnutrition, is best known for its ability to extend lifespan, improve metabolic fitness and increase stress resistance (Colman et al., 2009; Fontana et al., 2010; Hine et al., 2015). DR regimens, which vary widely, can emphasize either restriction of total food intake (calorie restriction, CR) or dilution of specific nutrients in the diet, such as the sulfur amino acids (SAA) methionine (M) and cysteine (C) (methionine restriction, MR) (Miller et al., 2005; Orentreich et al., 1993). We recently reported that CR increases hepatic CGL expression, endogenous H_2S production capacity and resistance to hepatic ischemia reperfusion injury, and that these are abrogated by dietary C excess (Hine et al., 2015). CR also promotes revascularization and recovery from femoral artery ligation in rodents (Kondo et al., 2009), and maintains vascular health in rodents and non-human primates in part by preserving capillary density in skeletal muscle (Omodei and Fontana, 2011). Interestingly, SIRT1 is activated in some tissues upon DR (Cantó and Auwerx, 2009; Wang, 2014) and required for VEGF-dependent angiogenesis (Potente et al., 2007). However, the effects of DR on angiogenesis and the potential role of H_2S remain unknown. Here, we identified SAA restriction as a proangiogenic trigger in EC *in vitro* and in skeletal muscle in mice *in vivo*.

Results

SAA restriction induces endothelial VEGF expression *in vitro* and functional angiogenesis *in vivo*

We tested the potential of isolated nutrient restriction independent of ischemia or hypoxia to impact angiogenesis *in vitro* using a model of SAA restriction (Hine et al., 2015). Human umbilical vein endothelial cell (HUVEC) cultured overnight in media lacking SAA (-M&C) displayed increased VEGF mRNA expression and protein secretion into the media (Fig. 1A).

This correlated with increased proangiogenic potential, including migration across a scratch (Fig. 1B); formation of capillary-like structures (tube formation, Fig. 1C); and increased sprout length in 3-dimensional HUVEC spheroid cultures, an effect that was abrogated by the specific VEGFR2 inhibitor SU5416 (Fig. 1D). Inhibiting SIRT1 activity with Ex-527 significantly reduced HUVEC tube formation (Fig. 1C) and branch point number (Fig. S1A) upon -M&C, suggesting that the proangiogenic pathway triggered by -M&C is dependent on both VEGF and SIRT1 activity.

To test the impact of dietary SAA restriction on angiogenesis *in vivo*, mice were given *ad libitum* access to an MR diet containing a limiting amount of M and lacking C (Miller et al., 2005; Orentreich et al., 1993). Young adult wildtype (WT) mice on MR for 2mo maintained a lower body weight despite normal food intake relative to mice fed a control diet containing normal M and C levels (Fig. S1B).

Strikingly, MR resulted in increased vascular density in skeletal muscle as determined by immunostaining (Fig. 1E) and flow cytometric analysis (Fig. S1C) for the EC marker CD31. Consistent with VEGF dependence, this effect was blocked by axitinib, one of the best characterized VEGF receptor inhibitors *in vivo* with demonstrated antiangiogenic activity in the context of tumor neovascularization (Ma and Waxman, 2008) (Fig. 1E, S1C). Interestingly, although expression of VEGF mRNA was not consistently affected upon MR in whole gastrocnemius muscle (Fig. S1D), there was a trend toward increased VEGF protein in gastrocnemius muscle extracts (Fig. S1E). VEGF and CD31 co-localized in gastrocnemius muscle by IHC (Fig. S1F) consistent with EC as the source of VEGF upon MR *in vivo* as observed upon -M&C *in vitro* (Fig. 1A).

Functional significance was tested in the context of femoral artery ligation in mice preconditioned on MR or control diets for 1mo prior to surgical occlusion, and returned to a complete diet after surgery (Fig. S1G). Although blood flow was similarly interrupted in both diet groups immediately after ligation (d0), return of blood flow indicative of neovascularization was accelerated in MR mice, with significant improvement by d3 after ligation (Fig. 1F). CD31 immunohistochemistry of muscle sections confirmed a relative increase in capillary density in both ischemic and non-ischemic legs of MR vs. control mice despite a return to a complete diet for 10d (Fig. 1G). Functional improvement was also observed in mice preconditioned on a different DR regimen, 40% calorie restriction (CR), for 1mo prior to femoral ligation (Fig. S1H–I). In addition to improved return of blood flow (Fig. S1H), CR mice also demonstrated improved treadmill exercise endurance testing on d4 after ligation (Fig. S1I). Together, these data suggest neovascularization induced by DR (in the form of CR or MR) as a contributing factor in the improved physiological response to acute blood flow cessation.

GCN2-dependent, hypoxia-independent regulation of VEGF and angiogenesis upon SAA restriction

Although HIF1α upon hypoxia is the best-characterized trigger of VEGF expression in multiple cell types including EC, VEGF expression upon -M&C was unaffected by HIF1α RNAi knockdown (KD) (Fig. 2A, S2A) and coincided with a trend towards reduced HIF1α protein expression (Fig. 2B, S2B). PGC1α can also induce VEGF independently of HIF1α

upon total nutrient/growth factor deprivation in myocytes but not EC (Arany et al., 2008). Consistent with this, endogenous PGC1α mRNA expression in HUVEC was very low as judged by Ct value (data not shown) and unaffected by -M&C (Fig. S2C), while exogenous PGC1α overexpression in HUVEC failed to modulate VEGF expression (Fig. S2D–E).

The AA starvation response (AASR), a branch of the ISR involving binding of uncharged cognate tRNAs to the general control nonderepressible 2 (GCN2) kinase, phosphorylation of eukaryotic translation initiation factor 2α (eIF2α) and translational derepression of ATF4 (Kilberg et al., 2005; Wek et al., 1995), has been implicated in DR-mediated resistance to ischemia reperfusion injury (Peng et al., 2012), but has not been assessed in EC. In HUVEC, - M&C increased eIF2α phosphorylation, ATF4 protein expression and transcription of the ATF4 target, Asns (Fig. 2B, S2B, F). ATF4 siRNA (Fig. S2G) reduced VEGF and Asns transcriptional upregulation upon -M&C (Fig. 2C, S2F), while ATF4 overexpression increased VEGF and Asns mRNA expression (Fig. 2D, S2G–I) and VEGF secretion into the media (Fig. 2E) independent of nutrient deprivation.

The requirement for GCN2 was tested in primary EC isolated from WT and GCN2KO mice (Fig. S2J). Similar to HUVEC, -M&C significantly increased VEGF and Asns mRNA expression (Fig. 2F, S2K) and sprout length (Fig. 2G) in WT but not GCN2KO EC. *In vivo,* GCN2KO mice failed to increase vascular density upon 2–4wk of MR compared to controls (Fig. 2H).

-M&C also increased VEGF expression in primary mouse dermal fibroblasts (MDF), immortalized mouse embryonic fibroblasts (MEF) and C2C12 myotubes (Fig. 2I). In primary skeletal myotubes, VEGF induction upon -M&C required GCN2 (Fig. 2J). In MDF, ATF4 shRNA prevented the increase in VEGF mRNA by -M&C (Fig. S2L). In C2C12 myotubes, VEGF induction coincided with increased eIF2α phosphorylation, ATF4 expression and reduced HIF1α protein levels (Fig. 2K). Notably, VEGF induction upon -M&C in C2C12 myotubes was unaffected by HIF1α RNAi KD under normoxic (20%) or hypoxic (<1%) oxygen tensions (Fig. S2M–O). PGC1α RNAi KD also failed to dampen VEGF induction upon -M&C in C2C12 myotubes (Fig. S2P).

Taken together, these data reveal SAA restriction and the GCN2/ATF4-dependent AASR as a novel trigger of increased VEGF expression and angiogenesis independent of hypoxia, HIF1α or PGC1α.

VEGF signalling and AASR converge on endothelial H_2S production by CGL

VEGF promotes angiogenesis in part by stimulating CGL-dependent production of the proangiogenic gas H_2S in EC (Papapetropoulos et al., 2009), however mechanisms of CGL regulation in EC and the importance of H_2S in angiogenesis remain poorly understood. H_2S production capacity (Fig. 3A) and endogenous H_2S levels (Fig. 3B) were similarly increased by - M&C and exogenous VEGF addition, and sensitive to the CGL inhibitor propargylglycine (PAG). -M&C also boosted endogenous H_2S production in primary hepatocytes, while VEGF did not because hepatocytes lack VEGFR2 (Fig. S3A).

CGL is an ATF4 target downstream of the ISR triggered either by ER stress in MEF (Dickhout et al., 2012) or cysteine deprivation in HepG2 (Lee et al., 2008). In primary mouse EC, CGL mRNA was strongly induced upon -M&C. (Fig. 3C). This effect was abrogated in EC lacking GCN2 (Fig. 3C) or in HUVEC upon ATF4 knockdown (Fig. 3D, S2F), while ATF4 overexpression increased CGL independent of SAA deprivation (Fig. 3E). Importantly, VEGF mRNA was not affected by the absence of CGL (Fig. S3B) *in vitro*, consistent with CGL and VEGF as independent downstream targets of the AASR. Interestingly, exogenous VEGF increased CGL mRNA (Fig. S3C) and protein (Fig. S3D) expression in EC independent of nutrient deprivation, suggestive of a positive feedback loop between VEGF and CGL expression, but without affecting expression of the two other H_2S-generating enzymes, CBS or 3-MST.

The functional relevance of endothelial CGL in angiogenic potential *in vitro* was assessed in the EC spheroid assay. Increased sprout length of EC spheroids upon -M&C was prevented by the CGL inhibitor PAG in HUVEC (Fig. 3F) and in CGLKO mouse EC (Fig. 3G). Thus, CGL is required for angiogenesis induced by -M&C *in vitro*.

CGL required for angiogenesis *in vivo*

We next tested the requirement for CGL-derived H_2S in angiogenesis triggered by MR *in vivo*. Consistent with CGL as the major H_2S producer in EC *in vivo* (Wang, 2012), P3 fluorescence indicative of endogenous H_2S production co-localized with $CD31^+$ cells in fresh-frozen sections of gastrocnemius muscle from WT but not CGLKO mice (Fig. 4A). Quantification of P3 intensity in WT and CGLKO mice fed Ctrl vs. MR diets for 2wk confirmed a CGL-dependent increase in EC H_2S production upon MR *in vivo* (Fig. 4B). Coincident with failure to increase H_2S, CGLKO mice failed to increase capillary density upon MR *in vivo* relative to WT mice (Fig. 4C). Furthermore, the CGL inhibitor PAG partially prevented 40% CR from improving recovery from femoral ligation (Fig. S1H–I). Taken together, these data are consistent with a requirement for CGL-derived H_2S for angiogenesis triggered by nutrient deprivation.

We next asked if CGL-derived H_2S is sufficient to promote angiogenesis independent of SAA restriction. To this end, we injected CGL-expressing adenovirus into the gastrocnemius muscle of WT mice via intra-muscular injection, likely resulting in CGL overexpression in both myotubes and EC due to the ability of the Ad5 serotype to infect multiple cell types. Local CGL viral transduction increased muscle H_2S production capacity (Fig. S4A) and vascular density (Fig. 4D) independent of any other proangiogenic stimulus, suggesting that an increase in CGL-derived H_2S is sufficient to trigger angiogenesis.

To test this apparent general requirement for CGL in angiogenesis independent of the upstream stimulus, we induced angiogenesis by either treadmill exercise training or by VEGF overexpression via intra-muscular injection of VEGF-overexpressing (ad-$VEGF_{165}$) adenovirus. Exercise training increased endogenous VEGF mRNA expression in WT mice (Fig. S4B), while both exercise training (Fig. 4E) and local VEGF overexpression via adenoviral gene delivery (Fig. 4F) increased capillary density in WT but not CGLKO mice. Taken together, these data indicate that CGL is necessary for VEGF-mediated neovascularization *in vivo* independent of the upstream proangiogenic stimulus.

H_2S promotes glucose uptake and ATP generation by glycolysis for EC migration

Because CGL is a promiscuous enzyme that can convert cystathionine to C as part of the transsulfuration pathway, but can also use C to produce H_2S and serine, we sought more direct evidence of H_2S as the CGL metabolite relevant to angiogenesis. H_2S addition to standard EC media in the form of NaHS increased proliferation (Fig. S5A) and migration across a scratch wound (Fig. 5A). This latter effect was only partially blocked with mitomycinC (MitoC), consistent with migration as a critical factor in H_2S-induced proangiogenic potential. In support of this, HUVEC overexpressing CGL (Ad-CGL) formed lamellipodial projections over larger areas (Fig. 5B) coincident with increased migration speed and greater cell body displacement (Fig. 5C).

Cell migration requires rapid ATP generation to facilitate actin cytoskeleton rearrangement, which in EC is met by increasing glycolytic metabolism (De Bock et al., 2013; Schoors et al., 2014). We thus examined glucose uptake and glycolytic ATP production as a function of genetic and pharmacological H_2S modulation. Treatment for 30min with NaHS increased glucose uptake in HUVEC similar to VEGF (Fig. 5D). Interestingly, H_2S-induced glucose uptake was independent of SIRT1 in mouse EC (Fig. S5B).

Glycolytic activity was assessed using several methods. Extracellular acidification rate (ECAR), a surrogate marker of glycolysis, was increased by NaHS treatment in HUVEC (Fig. S5C). In primary EC from WT mice, NaHS and VEGF increased ECAR to a similar level (Fig. 5E, S5D), while in CGLKO EC, ECAR was significantly reduced at baseline, and increased by NaHS but not VEGF administration (Fig. 5E). Interestingly, accumulation of the end product of aerobic glycolysis, lactate, in the media following NaHS treatment did not reach the level of statistical significance (Fig. S5E). We thus measured glycolysis directly using the release of ^3H_2O from C5-^{3}H-glucose and found a significant increase upon NaHS or VEGF treatment (Fig. 5F) beginning after 30min (Fig. S5F).

Consistent with increased glycolysis, H_2S boosted intracellular ATP levels over a rapid time course similar to exogenous VEGF (Fig. 5G). Both exogenous H_2S addition and CGL overexpression also increased EC migration, and this was sensitive to competitive inhibition of glycolysis by 2-deoxy-D-glucose (2DG; Fig. 5H–I). Together, these data support the functional relevance of CGL-derived H_2S in activation of glycolytic ATP generation necessary for proangiogenic migratory behaviour.

Steady-state flux analysis was employed to better understand glucose disposal upon NaHS treatment. Addition of ^{13}C1,2-glucose to the media for the final 15min of a 2hr NaHS treatment revealed significant changes in labeling of glycolytic intermediates, including an increase in glyceraldehyde-3-phosphate, dihydroxy-acetone-phosphate and fructose-phosphate (Fig. 5J). Interestingly, a significant increase was also observed in pentose phosphate pathway (PPP) and purine biosynthetic intermediates, including sedoheptulose-7P, phosphoribosyl-1- pyrophosphate and IMP (Fig. 5J). A significant increase in total unlabelled glycolytic and nucleotide metabolites was also observed (Fig. S5G). Increased glucose flux through the PPP is required for angiogenesis (Bierhansl et al., 2017; Vizan et al., 2009) and could also contribute to increased ECAR via CO_2 release

during the oxidative phase of the reaction (Fig. 5E, S5C), but is not mutually exclusive with the observed increase in glycolytic ATP generation.

Finally, we asked if NaHS and M&C removal triggered similar metabolic responses as predicted if endogenous H_2S production upon -M&C is important for its proangiogenic action. To this end, we performed unbiased metabolomic analyses of HUVEC cultured under standardized media conditions (complete DMEM supplemented with dialyzed FBS and EC growth factors) for 1hr before addition of NaHS addition or M&C removal. A comparison of global profiles over a time course following treatment revealed a time-dependent shift upon -M&C away from the control and a striking convergence after 4hr with the 15min NaHS profile (Fig. 5K). An analysis of all significant changes in the same direction between the 15min NaHS and -M&C groups included glycolytic and PPP intermediates (Fig. 5L).

H_2S shifts oxidative/glycolytic balance concomitant with inhibition of mitochondrial OXPHOS

By what mechanism does H_2S promote glucose uptake and disposal in EC? Increased ECAR by NaHS was unaffected by axitinib or the eNOS competitive antagonist L-nitroarginine methyl ester (L-NAME) (Fig. S5H). Similarly, NaHS-induced EC migration was unaffected by L-NAME (Fig. S5I) or genetic eNOS knockdown (Fig. S5J–K), together suggesting a mechanism of action either independent or downstream of proximal VEGFR2 signalling.

In many cell types, inhibition of mitochondrial oxidative phosphorylation (OXPHOS) and transient ATP depletion initiates adaptive responses including AMPK activation that boost glucose uptake and glycolytic ATP production (Hardie et al., 2016). At high concentrations, H_2S can inhibit complex IV of the mitochondrial ETC and prevent ATP generation by OXPHOS (Smith et al., 1977), however whether this mechanism of action contributes to its proangiogenic effect is unknown. Despite the fact that EC rely predominantly on glycolysis (De Bock et al., 2013), we observed significant changes in glucose flux through the citric acid cycle (reduced citrate/isocitrate and oxaloacetate, Fig. 5J) as well as reduced total citrate (Fig. S5G) suggesting a block in mitochondrial OXPHOS without an increase in cell death (Fig. S5L). Interestingly, labeled and total malate were increased in the same analyses, possibly due to an increase in the cytoplasmic pool, which cannot be distinguished from the mitochondrial pool in whole cell lysates.

CGLKO EC displayed increased oxygen consumption rate (OCR) under basal conditions relative to WT cells (Fig. 6A), consistent with the ability of endogenous H_2S to inhibit mitochondrial ETC activity. Similarly, exogenous H_2S decreased OCR concomitant with an increase in ECAR to the same levels as the Complex V inhibitor oligomycin (Fig. 6B). To confirm the predicted effects of H_2S on Complex IV activity, OCR was measured in isolated HUVEC mitochondria in the presence of NaHS or the Complex IV inhibitor KCN. In addition to the expected decrease in OCR in the presence of the Complex IV substrate TMPD-ascorbate, NaHS also reduced oxygen consumption fueled by pyruvate, consistent with additional ETC inhibition at Complex I (Fig. 6C).

We next asked if Complex IV inhibition was sufficient to trigger AMPK activation in EC. AMPK was activated within 5min of NaHS or KCN treatment (Fig. 6D–E) and returned to

baseline after 30min. Treatment with an AMPK inhibitor (Compound C) prevented the increase in ECAR (Fig. 6F), glucose uptake and migration (Fig. S6A–B). Consistent with the rapid and transient nature of AMPK activation, 10min NaHS treatment was sufficient to promote EC migration during the subsequent 12hr period, and this was blocked by Compound C (Fig. S6C–D).

To determine if energy stress was the proximal trigger to AMPK activation, we measured ATP/ADP ratio over a time course following NaHS addition, as well as energy charge 15min after NaHS addition, but observed no significant changes (Fig. S6E–F). AMPK can also be activated by upstream kinases such as CamKKβ (Lee et al., 2012) or reactive oxygen species (ROS) upon hypoxia (Emerling et al., 2009) or nutrient/energy deprivation (Li et al., 2013). However, NaHS-mediated glucose uptake was unaffected by the CamKKβ inhibitor STO-609 (Fig. S6G), while mitochondrial ROS failed to increase upon NaHS or KCN treatment (Fig. S6H).

Nonetheless, if inhibition of mitochondrial ATP synthesis is the trigger by which H_2S promotes AMPK activation, glycolytic ATP production and angiogenesis, then any ETC inhibitor should have similar proangiogenic effects. Consistent with this hypothesis, multiple ETC inhibitors targeting different complexes, as well as the uncoupler FCCP, increased glucose uptake (Fig. 6G), albeit with slightly different kinetics (Fig. S6I). ECAR (Fig. 6H, S6J) and glycolytic flux (Fig. S6K) were also stimulated by OXPHOS inhibition. Finally, multiple ETC inhibitors stimulated 2DG-sensitive EC migration (Fig. 6I, S6L). Together, these data are consistent with a mechanism of H_2S action in angiogenesis involving transient inhibition of mitochondrial respiration by direct inhibition of ETC, resulting in increased glucose uptake and a shift from oxidative phosphorylation to glycolysis and PPP.

Discussion

SAA restriction as a proangiogenic trigger

A model for the proangiogenic pathway activated by SAA restriction and controlled by the GCN2/ATF4-dependent AASR independent of hypoxia, HIF1α or PGC1α in EC is presented in Fig. 7. While ATF4 regulation of VEGF expression has been reported in the context of the ISR activated by AA deprivation or ER stress in a human retinal pigmented epithelial cell line *in vitro* (Abcouwer et al., 2002) or by mutation of tRNA synthetase genes in zebrafish *in vivo* (Castranova et al., 2016), it has not been previously linked to SAA deprivation via GCN2 in EC. ATF4 can also activate CGL and H_2S production, which can feed back to increase eIF2α phosphorylation and further activate the ISR (Yadav et al., 2017). Future studies will be required to determine the impact of AA deprivation on other proangiogenic factors such as FGF, and if there is any specificity to SAA. Furthermore, while ATF4 can activate VEGF and CGL expression in multiple different primary cell types *in vitro*, it remains to be determined which cell types *in vivo* are critical for the proangiogenic effects of SAA restriction.

Although H_2S can also be generated by other enzymes including CBS or 3-MST, we found a genetic requirement for CGL in angiogenesis triggered by nutrient deprivation, exercise or VEGF injection (Fig. 4). CGL is also critical for *de novo* C biogenesis via TSP, linking

methionine cycle metabolites upstream to glutathione and taurine production downstream, perturbation of any of which could potentially contribute to the observed effects. Finally, we acknowledge the apparent paradox of increased endogenous H_2S production in response to restriction of its substrate, C. However, as the source of free C for H_2S generation by CGL is not currently known, it could come from pools distinct from diet-derived or *de novo*-produced C. For example, cytoplasmic glutathione levels which are in the mM range could be utilized as a source of free C, as could products of proteosomal protein degradation or lysosomal autophagy. In support of this latter notion, the increase in H_2S production induced by growth factor (serum) withdrawal in cultured cells is partially abrogated by genetic or pharmacological inhibition of autophagy (Hine et al., 2017), while the benefits of MR on longevity in yeast require autophagy (Ruckenstuhl et al., 2014).

In an accompanying manuscript, Das et al. report an interaction between H_2S and SIRT1 in the regulation of angiogenesis as evidenced by the ability of H_2S/NMN supplementation in old mice to reverse age-associated loss of muscle vascular density and improved exercise performance (Das et al.). Although the mechanism by which H_2S augments SIRT1 function remains to be elucidated, these data suggest that H_2S and SIRT1 function in a critical axis regulating angiogenesis with the potential to mitigate or reverse oxidative stress-induced and aging-related changes in vascular health using pharmacological agents.

Mechanisms of H_2S regulation of energy metabolism in EC

H_2S at physiological levels is thought to exert its biological activities through non-mutually exclusive mechanisms, including post-translational modification of target proteins via S-sulfhydration of surface-exposed C residues (Mishanina et al., 2015; Mustafa et al., 2009); direct or indirect antioxidant action (Whiteman et al., 2004; Whiteman et al., 2005); or ATP generation via transfer of electrons to the mitochondrial SQR protein (Goubern et al., 2007; Yong and Searcy, 2001). There is clearly precedent for the potential of H_2S to regulate angiogenesis via S-sulfhydration of target proteins in multiple pathways implicated in angiogenesis, ranging from VEGFR2 signalling (Altaany et al., 2014; Coletta et al., 2012; Tao et al., 2013) to cellular energy metabolism via activation of the rate-limiting glycolytic enzyme GAPDH (Mustafa et al., 2009).

H_2S can also inhibit terminal electron transfer to oxygen (Nicholls and Kim, 1982) at supraphysiological levels, estimated to be greater than 20μM upon acute treatment of intact human colon carcinoma epithelial cells (Leschelle et al., 2005). Our data are consistent with the potential relevance this mechanism in regulation of EC oxidative/glycolytic energy balance, although whether levels of endogenously-generated H_2S upon SAA deprivation here or in other contexts reach this inhibitory concentration remains unclear (Cooper and Brown, 2008). Consistent with our findings in EC, an increase in H_2S in pancreatic β cells exposed to ER stress promotes aerobic glycolysis associated with decreased OXPHOS and S-sulfhydration of enzymes involved in energy metabolism (Gao et al., 2015). Interestingly, a number of tumors and cancer cells lines also upregulate GCN2 (Lehman et al., 2015; Wang et al., 2013) or H_2S production (Bhattacharyya et al., 2013; Sen et al., 2015; Sonke et al., 2015; Szabo et al., 2013), possibly contributing to the Warburg effect through inhibition of mitochondrial respiration.

STAR Methods

CONTACT FOR REAGENT AND RESOURCE SHARING

Further information and requests for resources and reagents should be directed to and will be fulfilled by the Lead Contact, James R. Mitchell (jmitchel@hsph.harvard.edu)

EXPERIMENTAL MODELS

Mice—All experiments were performed with the approval of the Harvard Medical Area or Boston University Institutional Animal Care and Use Committee (IACUC). 8–14wk old male or female C57BL/6 mice (The Jackson Laboratory, Bar Harbor, ME) were used for all experiments unless otherwise indicated. Male and female CGL WT and KO mice on a mixed 129/C57BL/6 background (Yang et al., 2008) and GCN2KO and control mice on a C57BL/6 background (Peng et al., 2012) were bred at our facility. Except where indicated, animals were maintained under standard group housing conditions with *ad libitum* access to food (Purina 5058) and water, 12-hr light/12-hr dark cycles, temperature between 20–23°C with 30–70% relative humidity.

Experimental diets were based on Research Diets D12450B with approximately 18% of calories from protein (hydrolyzed casein or individual crystalline amino acids (Ajinomoto) in the proportions present in casein), 10% from fat and 72% from carbohydrate. MR diets containing 1.5g methionine (M)/kg food and lacking cysteine (C) (Miller et al., 2005) in the context of a 14% protein/ 76% carbohydrate calorie diet were provided AL. In MR experiments with WT and CGLKO mice, the control diet was supplemented with 4.3g C/kg food to compensate for the inability of CGLKO mice to make C. AL food intake/g body weight was monitored daily for several days and used to calculate calorie restriction (CR) based on initial animal weights. Animals were fed daily with fresh food between 6–7pm.

Where indicated, axitinib was supplemented at a daily dose of ~30mg/kg/d in the food as previously described (Alonso et al., 2010; Ma and Waxman, 2008); and PAG was dosed once daily i.p. (10mg/kg) for the indicated time.

Cell Lines and Primary Tissue Culture Studies—Pooled human umbilical vein endothelial cells (HUVEC) were obtained from Lonza (C2519A, Lonza) and used between passage 1 and 7. HUVEC were cultured in endothelial basal medium (EBM-2) supplemented with 2%FBS and endothelial growth medium SingleQuots (Clonetics, Lonza) at 37°C in a humidified, multigas incubator (Napco Series 8000 WJ, Thermo Scientific) at 5%CO_2 and 3%O_2 achieved by displacing air with nitrogen gas.

Primary mouse endothelial cells were isolated from the lung by collagenase digestion (Liberase, Roche) followed by sequential affinity selection method using Dynabeads™ goat anti-rat conjugated to rat-anti mouse CD31 (BD Biosciences, San Jose, CA), and cultured in endothelial basal medium (EBM-2) supplemented with 2%FBS and endothelial growth medium SingleQuots (Clonetics, Lonza) at 37°C, 5%CO_2 and 3%O_2. At least 3 independent primary mouse EC cultures/genotype was tested per experiment.

Primary mouse hepatocytes were isolated by collagenase digestion, Percoll (GE Healthcare) gradient centrifugation and cultured in William's E media (Sigma) with 5%FBS at 37°C, 5%CO_2 and 3%O_2.

Primary mouse dermal fibroblasts (MDF) were obtained from tail skin of wildtype mice following collagenase digestion and cultured in DMEM with 10%FBS at 37°C, 5%CO_2 and 3%O_2.

Primary mouse skeletal myotubes were isolated from leg skeletal muscle following collagenase/dispase digestion and cultured in Ham's F12 with 20%FBS and 10ng/mL bFGF for approximately one week, then switched to Ham's F12 supplemented with 4% horse serum but lacking bFGF for 7d at 37°C in 5%CO_2 at normoxia (20%O_2).

C2C12 myoblasts were cultured in DMEM with 10%FBS until they reached 90% confluence, then switched to DMEM supplemented with 4% horse serum for 7d at 37°C in 5%CO_2 at normoxia (20%O_2).

Immortalized mouse embryonic fibroblasts (MEF) were cultured in DMEM with 10%FBS at 37°C in 5%CO_2 at normoxia (20%O_2).

The following methionine and cysteine deprivation conditions (-M&C) were used to simulate methionine restriction *in vitro*. For primary EC, when cultures reached confluence, the media was removed and replaced either with complete DMEM +/−M&C plus Glutamax (no pyruvate) (Sigma) supplemented with the same amount (2%) of dialyzed FBS and endothelial growth medium SingleQuots (Clonetics, Lonza) for 1 to 24hr. For hepatocytes, MDF, primary or C2C12 myotubes and MEF cultures, the media was removed and replaced with complete DMEM +/−M&C (plus Glutamax, no pyruvate; Sigma) supplemented with dialyzed FBS (10% for hepatocytes, MDF and MEF; 4% for the primary skeletal muscle and C2C12 myotubes)

Where indicated, media was supplemented with L-NAME (100μM), NaHS (100μM), PAG (100μM), SU5416 (20μM), axitinib (10μM), Ex527 (10μM), 2DG (1mM or 50mM), Compound C (10μM) or STO-609 (5μg/mL). Hypoxia was induced via air displacement with nitrogen gas.

METHOD DETAILS

Intramuscular adenoviral-mediated gene delivery—Local overexpression of CGL or VEGF in gastrocnemius was accomplished by intramuscular injection of 40μl containing a total of 10^9 PFU of an adenovirus-type 5 (dE1/E3) containing the CMV promoter driving expression of the mouse CGL gene (Ad-mCTH/CGL, Genbank RefSeq BC019483, ADV-256305 Vector Biolabs) or the human VEGF gene (Ad-hVEGFA165 Genbank RefSeq NM_001171626, Vector Biolabs) or the negative control virus Ad-CMV-Null (1300 Vector Biolabs) once weekly for 2wk.

Hindlimb ischemia model—12wk old C57BL/6 WT mice were anaesthetized with isoflurane and body temperature maintained on a circulating heated water pad. Following a 1cm groin incision, the neurovascular pedicle was visualized under a microscope (LW

Scientific, Z2 Zoom Stereoscope) and the femoral nerve carefully dissected out. The femoral vein (located medially) was separated from the femoral artery (located laterally) allowing electrocoagulation of the left common femoral artery, proximal to the bifurcation of superficial and deep femoral artery while sparing the vein and nerve. Once the artery was occluded, the surgical site was inspected for any residual bleeding (Hoefer et al., 2004; Mirabella et al., 2011).

Laser Doppler perfusion imaging—Laser Doppler perfusion imaging (LDPI) was performed as described previously (Hoefer et al., 2004; Mirabella et al., 2011). Briefly, mice were kept under isoflurane anesthesia, and body temperature maintained on a circulating heated water pad. Blood flow recovery was monitored at d 0 (immediately post-surgery), d1, d3, and d10 using an LDPI analyzer (Moor Instruments, Inc. DE). The LDPI intensity of the ischemic foot was normalized to the contralateral foot and represented as relative blood flow of the ischemic limb (Ischemic/Non-ischemic ratio). AUCs from I/NI ratios from each animal over time were used for statistical comparisons between groups.

Treadmill exercise training—Twelve wk old male WT and CGLKO mice were randomized into sedentary or exercise groups. Mice were acclimatized to the treadmill (Columbus Instruments 6 lane treadmill) at 8 m/min for 5min for 3d prior to exercise training. Mice ran 30min/d at 5° incline at 12m/min for the first wk of training. Mice continued running 30min/d at 5° incline at 14m/min for an additional 3wk to reach 1mo total of exercise training. Sedentary controls and exercised animals were co-housed. Mice were euthanized 1hr after the final exercise bout (Narkar et al., 2008).

Treadmill exercise test—2 and 3d after ischemic injury, mice were acclimatized to the treadmill (Columbus Instruments 6 lane treadmill) at 8 m/min for 5min prior to exercise training. At d4, mice were run until exhaustion at 5° incline, 8m/min for 10min then 10m/min for 5min, with a 2m/min increase in speed every 5min (Narkar et al., 2008).

Gene expression analysis by qPCR—Total RNA was isolated from tissues and cells using RNeasy Mini Kit (Qiagen) and cDNA synthesized by random hexamer priming with the Verso cDNA kit (Thermo). qRT-PCR was performed with SYBR green dye (Lonza) and TaqPro DNA polymerase (Denville). Fold changes were calculated by the $\Delta\Delta C_t$ method (Livak and Schmittgen, 2001) using Hprt, 18S and/or β-Actin genes as standards, and normalized to the experimental control. Human primer sequences are indicated in the Key Resources Table, and mouse primer sequences are additionally found in Table S1.

Immunoblotting—Cells were homogenized with passive lysis buffer (Promega), normalized for protein content, boiled with SDS loading buffer and separated by SDS-PAGE. Proteins were transferred to PVDF membrane (Whatman) and blotted for CGL (ab151769 Abcam), HIF1α (10006421 Cayman Chemical), p-eIF2α Ser51 (9712S Cell Signaling), total eIF2α(9722S Cell Signaling), ATF4 (11815 Cell Signaling), Actin (13E5 Cell Signaling) and Tubulin (2146S Cell Signaling) and secondarily with HRP-conjugated anti-rabbit antibody (Dako).

VEGF ELISAs—Mouse and human VEGF ELISA kits were purchased from Peprotech (900-K99) and R&D System (DEV00), respectively, and assays performed according to manufacturer's instructions on 100µl of plasma or cell culture media per analysis. For analysis of VEGF protein in muscle, approximately 100mg of frozen gastrocnemius muscle was pulverized using a mortar and pestle, and the powder transferred to a 1.5mL microcentrifuge tube containing 150µL of PBS. The tissue was further disrupted using a mechanical tissue homogenizer (Kimble Kontes Pellet Pestle, Fisher Scientific). After three cycles of freezing and thawing, the tissue suspension was microcentrifuged at max speed for 10min and the supernatant recovered and stored at −80 °C. Lysates were adjusted to 0.5µg/µL in PBS and run using a mouse VEGF ELISA kit from R&D systems (MMV00) was used.

Immunohistochemistry and capillary density analysis—IHC was performed on frozen sections of unfixed gastrocnemius muscle (50µm for CD31 quantification; 20µm for CD31/VEGF/IB4 co-staining). After 5min fixation in PFA 4% and rinsing in PBS, immunostaining was performed as previously described (Longchamp et al., 2014). Primary antibodies included anti-mouse CD31 (BD Bioscience), anti-mouse VEGF (Novus Biologicals) and Isolectin B4 (Life Technologies) at a dilution of 1:100. For capillary density measurements, CD31 area was quantified from randomly photographed 10µm stack sections (6 images per section, 4 sections per muscle per mouse) using Fiji software (http://fiji.sc/Fiji). All quantifications were performed blindly.

CD31 FACS analysis—Following enzymatic digestion of muscle with collagenase/dispase mix, cells were blocked with mouse FcR blocking reagent (Miltenyl Biotech) and stained for 30min at 4 °C in the dark with CD31APC at 1:100 (BioLegend). Cells were washed and acquired immediately on an LSR II flow cytometer (BD Biosciences) and analyzed with FlowJo. CD31 positive endothelial cells are expressed as a percentage of total cells recovered from the enzymatically digested muscle cells as assessed by forward and side scatter.

H_2S measurements

Detection of H_2S production capacity in live cultures by lead sulfide method: For detection of H_2S production in live cells, growth media was supplemented with 10mM cysteine and 10µM pyridoxal 5'-phosphate hydrate (PLP, Sigma), and a lead 6x4 inch pieces of lead acetate paper, made by soaking 703 size blotting paper (VWR) in 20mM lead acetate (Sigma) and then vacuum drying, was placed over the plate for 2–24hr of further incubation in a CO_2 incubator at 37°C until lead sulfide was detected but not saturated.

Detection of endogenous H_2S with fluorescent P3 probe in cultured cells or frozen tissue sections: For detection of endogenous H_2S production in live adherent cells, growth media was supplemented with 10µM P3 probe (Singha et al., 2015) for 30min prior to fixation. Quantification was performed by calculating the average P3 signal intensity per cell. Cell areas were automatically segmented using brightfield images. Values presented are average P3 intensity per cell, corrected for total cell area. Analyses were performed using Matlab R2017A. For detection of endogenous H_2S production in tissue sections, 50µm

frozen sections of unfixed gastrocnemius muscle were incubated with 20μM P3 probe for 5min and washed 2X with PBS. Sections were then fixed for 5min in 4% PFA prior to immunostaining using a 2 photon microscope (Zeiss LSM780 w/ Mai Tai HP 2-photon laser (Spectra Physics) at 880nm excitation and 520–550nm emission (Singha et al., 2015).

Genetic manipulations in cultured cells

siRNA knockdown: siRNA knockdown of human activating transcription factor 4 (ATF4), human endothelial nitric oxide synthase (eNOS), human hypoxia-inducible factor 1-α (HIF1α), PGC1α (PPARGC1A) in HUVEC as well as mouse HIF1α and PGC1α in C2C12 myoblasts was performed using lipofectamine RNAiMAX (Life Technologies) and 30nM siRNA purchased from Ambion (Ambion, ThermoFisher) as described previously (Hine et al., 2015). All experiments were performed 2 d after transfection. Knockdown was confirmed by immunoblot and/or qPCR.

shRNA knockdown of ATF4: MDF were infected overnight in complete medium and collected 2d later using Ad-m-ATF4-shRNA or the negative control virus Ad-CMV-Null adenovirus amplified and purified by Vector Biolabs (Philadelphia, PA, U.S.A.).

ATF4 overexpression: ATF4 overexpression in HUVEC was performed using Lipofectamine 2000 (Life Technologies) and 1ug of prK-ATF4 plasmid per well (12-well format) overnight. All experiments were performed 2d after transfection. Overexpression was confirmed by immunoblot and/or qPCR.

Adenoviral-mediated CGL overexpression: HUVEC were infected overnight in complete medium and collected 2 d later using Ad-m-CTH or the negative control virus Ad-CMV-Null adenovirus amplified and purified by Vector Biolabs (Philadelphia, PA, U.S.A.).

Angiogenesis assays in vitro

Migration assay: EC were seeded at 100,000 cells per well in 24-well plate in EGM with 2% serum and growth factors (Lonza). ~12hr later, media was switched to EGM without serum/growth factors, and in some cases mitotically arrested (1μg/mL MitoC). A single scratch wound was created using a sterile p200 pipette tip on a confluent field of EC. Floating cells were washed away and EGM (or DMEM +/−M&C media) with dialyzed serum and growth factors replaced, including treatments. Repopulation/migration across the scratch wound was recorded by phase-contrast microscopy every 4hr for up to 20hr using a digital camera. Wound closure (gap area at t=Xhr relative to t=0hr) was determined at each time point from digital images using ImageJ software.

Tube formation: Formation of tube networks was assessed as described previously (Borradaile and Pickering, 2009). HUVEC were seeded at 10,000 cells per well in a 24-well plate (Corning) coated with 150 μL Cultrex reduced growth factor basement membrane extract (Trevigen). Following an 18 h-incubation, resulting tube networks were analyzed by light microscopy (Nikon Eclipse TiE). The total length of tubule networks and the number of branch points were quantified by ImageJ software.

Spheroid capillary sprouting assay: Hanging drops of HUVEC or primary mouse EC in EGM2 (De Bock et al., 2013) were embedded in Matrigel® (Corning) and cultured in the indicated media for 24hr to induce sprouting. Compounds were added at the indicated concentrations during the gel culture step, using corresponding vehicle concentrations as control. Spheroid cultures were stained with phalloidin diluted 1:500 in PBST for 1hr at RT and counterstained with DAPI. Images were captured with a Zeiss LSM 510 Meta NLO confocal microscope (oil objectives: x 40 with NA 1.3, x 63 with NA1.4, x 100 with NA 1.3; Carl Zeiss, Munich, Germany) or a Leica laser-scanning SP5 confocal microscope (Leica, Manheim, Germany). Analysis of the sprout length was performed using ImageJ software.

Proliferation—HUVEC were cultured to 60% confluency in a 12-well plate on glass coverslips, washed with PBS and incubated for 24hrs in EGM2 containing 0.1mM BrdU. Immunostaining was performed on cells washed and fixed for 5min in −20°C acetone, air - dried, rinsed in PBS and permeabilized for 1 h in PBS supplemented with 2% BSA and 0.1% Triton X-100. BrdU positive nuclei were automatically detected using the ImageJ software and normalized to the total number of DAPI-positive nuclei.

Glucose uptake—For VEGF and NaHS treatment +/− Compound C (10μM) (Fig. 5D, Fig. S6A), HUVEC were pretreated for 1hr with 50ng/ml VEGF (Peprotech) or 100μM NaHS. Cells were then depleted in Krebs-Ringer Bicarbonate Buffer (KRB; NaH_2PO_4/ Na_2HPO_4 10mM, NaCl 136mM, KCl 4.7mM, MgSO4 1.25mM, CaCl2 1.25mM, pH7.4), without glucose and serum for 30min and then incubated for 6min in a solution containing 0.5μCi ^{3}H-2DG. On ice, cells were then washed in cold PBS 3 times, lysed, and sample counted in a liquid scintillation counter. Samples were normalized to protein content as measured from the same cells by BCA. For remaining glucose uptake experiments (Fig. S5B, S6E, I), EC were treated with NaHS (100μM), KCN (10μM), Antimycin A (2.5μM), Oligomycin (2μM), or FCCP (1.5μM) for 45, 75 or 195min in EGM-2. When indicated, inhibitors were added 30min before the addition of the tracer. Fifteen min before the termination of the experiment, 0.4μCi of ^{3}H-2DG was added to each well (1mL final volume, 12-well format). At the end of the incubation the plate was rapidly transferred on ice, media removed and washed 4 times with PBS + BSA 0.1%. Finally, cell lysis was performed with NaOH 0.2% + SDS 0.5%. Lysate (500uL) was mixed with scintillation fluid (5mL) and sample radioactivity measured in a scintillation counter (Beckman).

Glycolytic flux analysis—HUVEC were cultured with the standard media (EGM-2), and stimulated for up to 3hr with test compounds (NaHS (100μM), VEGF (50ng/mL), Antimycin A (2.5μM), Oligomycin (2μM), or 2DG (1mM). 15min before the end of the incubation, 5uCi D-[5-3H(N)]-glucose was added to 1.5mL media (12-well format), then the plate was rapidly transferred on ice, and the media (1.5mL) transferred into a 5 mL vial. One PBS wash (1.5mL) was performed and liquid combined with media. The vial was inserted into a 50mL tube pre-filled with 3mL water. Tube was tightly capped and evaporation was performed at room temperature for 48hr. Finally, 2mL of water was collected from the 50mL tube and mixed with 10mL of scintillation fluid. Sample radioactivity measured in a scintillation counter (Beckman).

ATP and ATP/ADP ratio—Cells in a 96-well format were treated with NaHS, VEGF or 2DG in a reverse time course. ATP was measured by addition of 70μL of Cell TITER-Glo (Promega), plate incubated in the dark for 10min and luminescence quantified by a plate reader (BioTek instruments). ADP/ATP ratio was calculated after measuring ADP and ATP by a commercially available enzymatic assay (ApoSENSOR, BioVision), according to the manufacturer's instructions.

Energy charge—Steady-state mass spec measurements of AMP, ADP and ATP were used to calculate energy charge using the following equation: (ATP +1/2ADP)/(ATP + ADP + AMP).

Lactate—Lactate in HUVEC culture media was measured after 30min and 2hr of treatment with NaHS (100μM) or -M&C. The assay was performed using a plate-based colorimetric assay (Cell Biolabs Inc.) according to the manufacturer's protocol.

Cell death and ROS—Apoptosis and cell death was measured after 12hr treatment with NaHS (100μM) or – M&C using a FACS-based annexin V/propidium iodide assay according to the manufacturer's protocol (BD Biosciences).

Reactive oxygen species were measured after 15min, 1hr and 2hr incubations with NaHS (100μM), FCCP (2μM) or KCN (10μM). Menadione (10μM) was used as a positive control. Cells were stained for 15min with CellROX Green dye in the treatment media, fixed with 2% paraformaldehyde and measured using FACS.

Seahorse—Cellular oxygen consumption and extracellular acidification rate was measured using the Seahorse Cell Metabolism Analyzer XF96 (Seahorse Biosciences). Cells were plated at a density of 12,000 cells and untreated or pretreated with 100μM NaHS, 10μM KCN or 500μM phenformin for 2hr. After 24hr, media was changed to unbuffered XF assay media with 0 or 11mM glucose, 0 or 2mM glutamine and pyruvate at pH7.4 and basal OCR and ECAR measured for 5 blocks of 2min mixing and 5min measuring. Glucose (10mM final), 2DG (50mM final) and Oligomycin (2.5μM final) were injected at indicated times. All plates were normalized to protein content as measured from the same cells after Seahorse by BCA.

Mitochondrial respiration in permeabilized cells using complex-specific substrates was measured in a Seahorse Cell Metabolism Analyzer XF24 (Seahorse Biosciences) as previously described (Salabei et al., 2014). Briefly, cells were plated at a density of 100,000 cells in EGM- 2. Four hr later, cells were washed with MAS buffer, then incubated with MAS buffer containing 10mM pryruvate, 2mM malate, 4uM FCCP and 25ug/mL Saponin for 1hr, untreated or pretreated with 100μM NaHS or 10μM KCN. OCR was measured for 10 blocks of 1min mixing and 2min measuring. Rotenone (1μM final), Succinate (10mM final), Antimycin A (20μM final), and TMPD/Ascorbate (0.5mM/2mM final) were injected in order.

Metabolite profiling for glucose flux analyses—To determine the relative levels of intracellular metabolites, extracts were prepared and analyzed by LC/MS/MS. Triplicate 15-

cm confluent plates were incubated in EGM-2 media in presence or absence of 100μM NaHS 105min prior to extraction. For D-[1,2-^{13}C]-glucose flux studies, cells were washed once with serum- and glucose free DMEM and then incubated in DMEM containing a 10mM 1:1 mixture of D-[1,2-^{13}C]-glucose and unlabeled D-glucose for 15min. Metabolites were extracted on dry ice with 4-mL 80% methanol (−80°C), as described previously (Ben-Sahra et al., 2013). Insoluble material was pelleted by centrifugation at 3000*g* for 5min, followed by two subsequent extractions of the insoluble pellet with 0.5-mL 80% methanol, with centrifugation at 16,000*g* for 5min. The 5mL metabolite extract from the pooled supernatants was dried down under nitrogen gas using an N-EVAP (Organomation Associates, Inc.).

Dried pellets were resuspended using 20μL HPLC grade water for mass spectrometry. 10μL were injected and analyzed using a 5500 QTRAP triple quadrupole mass spectrometer (AB/SCIEX) coupled to a Prominence UFLC HPLC system (Shimadzu) via selected reaction monitoring (SRM). Some metabolites were targeted in both positive and negative ion mode for a total of 287 SRM transitions using pos/neg polarity switching. ESI voltage was +4900V in positive ion mode and –4500V in negative ion mode. The dwell time was 3ms per SRM transition and the total cycle time was 1.55 seconds. Approximately 10–14 data points were acquired per detected metabolite. Samples were delivered to the MS via normal phase chromatography using a 4.6mm i.d. x 10cm Amide Xbridge HILIC column (Waters Corp.) at 350μL/min. Gradients were run starting from 85% buffer B (HPLC grade acetonitrile) to 42% B from 0–5min; 42% B to 0% B from 5–16min; 0% B was held from 16–24min; 0% B to 85% B from 24–25min; 85% B was held for 7min to re-equilibrate the column. Buffer A was comprised of 20mM ammonium hydroxide/20mM ammonium acetate (pH=9.0) in 95:5 water:acetonitrile. Peak areas from the total ion current for each metabolite SRM transition were integrated using MultiQuant v2.0 software (AB/SCIEX). For stable isotope labeling experiments, custom SRMs were created for expected ^{13}C incorporation in various forms for targeted LC/MS/MS. Samples were quantile normalized and log transformed and metabolites were pareto scaled prior to analysis. Analyses were performed using R version 3.3.2.

Global metabolite profiling—HUVEC grown in EBM-2 media with BulletKit were switched to DMEM with 2% dialyzed FBS all non-serum BulletKit components. After a 1hr equilibration period, cells were switched to treatment media (control, -M&C, NaHS 100μM). After the treatment period (15min, 2hr, 4hr) cells were collected and analyzed for total metabolite profile by mass spectrometry using the methods detailed in the preceding section.

QUANTIFICATION and STATISTICAL ANALYSIS

Data are displayed as means +/− standard deviation (SD) and statistical significance assessed in GraphPad Prism using Student’s T test, 1-way or 2-way ANOVA unless otherwise specified. A P-value of 0.05 or less was deemed statistically significant.

Supplementary Material

Refer to Web version on PubMed Central for supplementary material.

Acknowledgments

We thank Florant Allagnat for critical discussions and reading the manuscript; Andrew Thompson, Nandan Nurukar and Rohan Kulkarni for technical assistance; Gokhan Hotamisligil for the use of the Seahorse; John Asara for assistance with metabolomics; and Constance Cepko for the use of the 2-photon microscope. This work was supported by grants from the Swiss National Science Foundation (P1LAP3_158895) to A.L.; National Science Foundation (NSF-DGE1144152) to L.E.B.; the Canadian Institutes of Health Sciences to R.W.; NIH (EB00262) to C.S.C.; American Heart Association (12GRNT9510001, 12GRNT1207025), Lea Carpenter du Pont Vascular Surgery Fund, and Carl and Ruth Shapiro Family Foundation to C.K.O.; and NIH (AG036712, DK090629) and Charoen Pokphand Group to J.R.M.

References

Abcouwer SF, Marjon PL, Loper RK, Vander Jagt DL. Response of VEGF expression to amino acid deprivation and inducers of endoplasmic reticulum stress. Invest Ophthalmol Vis Sci. 2002; 43:2791–2798. [PubMed: 12147617]

Alonso F, Krattinger N, Mazzolai L, Simon A, Waeber G, Meda P, Haefliger JA. An angiotensin II- and NF-kappaB-dependent mechanism increases connexin 43 in murine arteries targeted by renin-dependent hypertension. Cardiovasc Res. 2010; 87:166–176. [PubMed: 20110337]

Altaany Z, Ju Y, Yang G, Wang R. The coordination of S-sulfhydration, Snitrosylation, and phosphorylation of endothelial nitric oxide synthase by hydrogen sulfide. Sci Signal. 2014; 7:ra87. [PubMed: 25205851]

Arany Z, Foo SY, Ma Y, Ruas JL, Bommi-Reddy A, Girnun G, Cooper M, Laznik D, Chinsomboon J, Rangwala SM, et al. HIF-independent regulation of VEGF and angiogenesis by the transcriptional coactivator PGC-1alpha. Nature. 2008; 451:1008–1012. [PubMed: 18288196]

Ben-Sahra I, Howell JJ, Asara JM, Manning BD. Stimulation of de novo pyrimidine synthesis by growth signaling through mTOR and S6K1. Science. 2013; 339:1323– 1328. [PubMed: 23429703]

Bhattacharyya S, Saha S, Giri K, Lanza IR, Nair KS, Jennings NB, Rodriguez-Aguayo C, Lopez-Berestein G, Basal E, Weaver AL, et al. Cystathionine beta-synthase (CBS) contributes to advanced ovarian cancer progression and drug resistance. PLoS One. 2013; 8:e79167. [PubMed: 24236104]

Bierhansl L, Conradi LC, Treps L, Dewerchin M, Carmeliet P. Central Role of Metabolism in Endothelial Cell Function and Vascular Disease. Physiology (Bethesda). 2017; 32:126–140. [PubMed: 28202623]

Borradaile NM, Pickering JG. Nicotinamide phosphoribosyltransferase imparts human endothelial cells with extended replicative lifespan and enhanced angiogenic capacity in a high glucose environment. Aging Cell. 2009; 8:100–112. [PubMed: 19302375]

Cai WJ, Wang MJ, Moore PK, Jin HM, Yao T, Zhu YC. The novel proangiogenic effect of hydrogen sulfide is dependent on Akt phosphorylation. Cardiovasc Res. 2007; 76:29–40. [PubMed: 17631873]

Cantó C, Auwerx J. Caloric restriction, SIRT1 and longevity. Trends Endocrinol Metab. 2009; 20:325–331. [PubMed: 19713122]

Castranova D, Davis AE, Lo BD, Miller MF, Paukstelis PJ, Swift MR, Pham VN, Torres-Vazquez J, Bell K, Shaw KM, et al. Aminoacyl-Transfer RNA Synthetase Deficiency Promotes Angiogenesis via the Unfolded Protein Response Pathway. Arterioscler Thromb Vasc Biol. 2016; 36:655–662. [PubMed: 26821951]

Coletta C, Papapetropoulos A, Erdelyi K, Olah G, Módis K, Panopoulos P, Asimakopoulou A, Gerö D, Sharina I, Martin E, et al. Hydrogen sulfide and nitric oxide are mutually dependent in the regulation of angiogenesis and endothelium-dependent vasorelaxation. Proc Natl Acad Sci U S A. 2012; 109:9161–9166. [PubMed: 22570497]

Colman RJ, Anderson RM, Johnson SC, Kastman EK, Kosmatka KJ, Beasley TM, Allison DB, Cruzen C, Simmons HA, Kemnitz JW, et al. Caloric restriction delays disease onset and mortality in rhesus monkeys. Science. 2009; 325:201–204. [PubMed: 19590001]

Cooper CE, Brown GC. The inhibition of mitochondrial cytochrome oxidase by the gases carbon monoxide, nitric oxide, hydrogen cyanide and hydrogen sulfide: chemical mechanism and physiological significance. J Bioenerg Biomembr. 2008; 40:533–539. [PubMed: 18839291]

De Bock K, Georgiadou M, Schoors S, Kuchnio A, Wong BW, Cantelmo AR, Quaegebeur A, Ghesquiere B, Cauwenberghs S, Eelen G, et al. Role of PFKFB3-driven glycolysis in vessel sprouting. Cell. 2013; 154:651–663. [PubMed: 23911327]

Dickhout JG, Carlisle RE, Jerome DE, Mohammed-Ali Z, Jiang H, Yang G, Mani S, Garg SK, Banerjee R, Kaufman RJ, et al. Integrated stress response modulates cellular redox state via induction of cystathionine gamma-lyase: cross-talk between integrated stress response and thiol metabolism. J Biol Chem. 2012; 287:7603–7614. [PubMed: 22215680]

Emerling BM, Weinberg F, Snyder C, Burgess Z, Mutlu GM, Viollet B, Budinger GR, Chandel NS. Hypoxic activation of AMPK is dependent on mitochondrial ROS but independent of an increase in AMP/ATP ratio. Free Radic Biol Med. 2009; 46:1386–1391. [PubMed: 19268526]

Fontana L, Partridge L, Longo VD. Extending healthy life span--from yeast to humans. Science. 2010; 328:321–326. [PubMed: 20395504]

Fukumura D, Kashiwagi S, Jain RK. The role of nitric oxide in tumour progression. Nat Rev Cancer. 2006; 6:521–534. [PubMed: 16794635]

Gao XH, Krokowski D, Guan BJ, Bederman I, Majumder M, Parisien M, Diatchenko L, Kabil O, Willard B, Banerjee R, et al. Quantitative H2S-mediated protein sulfhydration reveals metabolic reprogramming during the integrated stress response. Elife. 2015; 4:e10067. [PubMed: 26595448]

Goubern M, Andriamihaja M, Nubel T, Blachier F, Bouillaud F. Sulfide, the first inorganic substrate for human cells. FASEB J. 2007; 21:1699–1706. [PubMed: 17314140]

Hardie DG, Schaffer BE, Brunet A. AMPK: An Energy-Sensing Pathway with Multiple Inputs and Outputs. Trends Cell Biol. 2016; 26:190–201. [PubMed: 26616193]

Hine C, Harputlugil E, Zhang Y, Ruckenstuhl C, Lee BC, Brace L, Longchamp A, Trevino-Villarreal JH, Mejia P, Ozaki CK, et al. Endogenous hydrogen sulfide production is essential for dietary restriction benefits. Cell. 2015; 160:132–144. [PubMed: 25542313]

Hine C, Kim HJ, Zhu Y, Harputlugil E, Longchamp A, Matos MS, Ramadoss P, Bauerle K, Brace L, Asara JM, et al. Hypothalamic-Pituitary Axis Regulates Hydrogen Sulfide Production. Cell Metab. 2017; 25:1320–1333. e1325. [PubMed: 28591635]

Hoefer IE, van Royen N, Rectenwald JE, Deindl E, Hua J, Jost M, Grundmann S, Voskuil M, Ozaki CK, Piek JJ, et al. Arteriogenesis proceeds via ICAM-1/Mac- 1- mediated mechanisms. Circ Res. 2004; 94:1179–1185. [PubMed: 15059933]

Katsouda A, Bibli SI, Pyriochou A, Szabo C, Papapetropoulos A. Regulation and role of endogenously produced hydrogen sulfide in angiogenesis. Pharmacol Res. 2016; 113:175–185. [PubMed: 27569706]

Kilberg MS, Pan YX, Chen H, Leung-Pineda V. Nutritional control of gene expression: how mammalian cells respond to amino acid limitation. Annu Rev Nutr. 2005; 25:59–85. [PubMed: 16011459]

Kolluru GK, Bir SC, Yuan S, Shen X, Pardue S, Wang R, Kevil CG. Cystathionine γ-lyase regulates arteriogenesis through NO dependent monocyte recruitment. Cardiovasc Res. 2015

Kondo M, Shibata R, Miura R, Shimano M, Kondo K, Li P, Ohashi T, Kihara S, Maeda N, Walsh K, et al. Caloric restriction stimulates revascularization in response to ischemia via adiponectin-mediated activation of endothelial nitric-oxide synthase. J Biol Chem. 2009; 284:1718–1724. [PubMed: 18990685]

Lee HJ, Mariappan MM, Feliers D, Cavaglieri RC, Sataranatarajan K, Abboud HE, Choudhury GG, Kasinath BS. Hydrogen sulfide inhibits high glucoseinduced matrix protein synthesis by activating AMP-activated protein kinase in renal epithelial cells. J Biol Chem. 2012; 287:4451–4461. [PubMed: 22158625]

Lee JI, Dominy JE Jr, Sikalidis AK, Hirschberger LL, Wang W, Stipanuk MH. HepG2/C3A cells respond to cysteine deprivation by induction of the amino acid deprivation/integrated stress response pathway. Physiol Genomics. 2008; 33:218–229. [PubMed: 18285520]

Lehman SL, Ryeom S, Koumenis C. Signaling through alternative Integrated Stress Response pathways compensates for GCN2 loss in a mouse model of soft tissue sarcoma. Sci Rep. 2015; 5:11781. [PubMed: 26123823]

Leschelle X, Goubern M, Andriamihaja M, Blottiere HM, Couplan E, Gonzalez-Barroso MD, Petit C, Pagniez A, Chaumontet C, Mignotte B, et al. Adaptative metabolic response of human colonic

epithelial cells to the adverse effects of the luminal compound sulfide. Biochim Biophys Acta. 2005; 1725:201–212. [PubMed: 15996823]

Li L, Chen Y, Gibson SB. Starvation-induced autophagy is regulated by mitochondrial reactive oxygen species leading to AMPK activation. Cell Signal. 2013; 25:50–65. [PubMed: 23000343]

Livak KJ, Schmittgen TD. Analysis of relative gene expression data using real-time quantitative PCR and the 2(−Delta Delta C(T)) Method. Methods. 2001; 25:402–408. [PubMed: 11846609]

Longchamp A, Alonso F, Dubuis C, Allagnat F, Berard X, Meda P, Saucy F, Corpataux JM, Déglise S, Haefliger JA. The use of external mesh reinforcement to reduce intimal hyperplasia and preserve the structure of human saphenous veins. Biomaterials. 2014; 35:2588–2599. [PubMed: 24429385]

Ma J, Waxman DJ. Modulation of the antitumor activity of metronomic cyclophosphamide by the angiogenesis inhibitor axitinib. Mol Cancer Ther. 2008; 7:79–89. [PubMed: 18202011]

Miller RA, Buehner G, Chang Y, Harper JM, Sigler R, Smith-Wheelock M. Methionine-deficient diet extends mouse lifespan, slows immune and lens aging, alters glucose, T4, IGF-I and insulin levels, and increases hepatocyte MIF levels and stress resistance. Aging Cell. 2005; 4:119–125. [PubMed: 15924568]

Mirabella T, Teodelinda M, Cilli M, Michele C, Carlone S, Sebastiano C, Cancedda R, Ranieri C, Gentili C, Chiara G. Amniotic liquid derived stem cells as reservoir of secreted angiogenic factors capable of stimulating neo-arteriogenesis in an ischemic model. Biomaterials. 2011; 32:3689–3699. [PubMed: 21371750]

Mishanina TV, Libiad M, Banerjee R. Biogenesis of reactive sulfur species for signaling by hydrogen sulfide oxidation pathways. Nat Chem Biol. 2015; 11:457–464. [PubMed: 26083070]

Mustafa AK, Gadalla MM, Sen N, Kim S, Mu W, Gazi SK, Barrow RK, Yang G, Wang R, Snyder SH. H2S signals through protein S-sulfhydration. Sci Signal. 2009; 2:ra72. [PubMed: 19903941]

Narkar VA, Downes M, Yu RT, Embler E, Wang YX, Banayo E, Mihaylova MM, Nelson MC, Zou Y, Juguilon H, et al. AMPK and PPARdelta agonists are exercise mimetics. Cell. 2008; 134:405–415. [PubMed: 18674809]

Nicholls P, Kim JK. Sulphide as an inhibitor and electron donor for the cytochrome c oxidase system. Can J Biochem. 1982; 60:613–623. [PubMed: 6288202]

Olsson AK, Dimberg A, Kreuger J, Claesson-Welsh L. VEGF receptor signalling - in control of vascular function. Nat Rev Mol Cell Biol. 2006; 7:359–371. [PubMed: 16633338]

Omodei D, Fontana L. Calorie restriction and prevention of age-associated chronic disease. FEBS Lett. 2011; 585:1537–1542. [PubMed: 21402069]

Orentreich N, Matias JR, DeFelice A, Zimmerman JA. Low methionine ingestion by rats extends life span. J Nutr. 1993; 123:269–274. [PubMed: 8429371]

Papapetropoulos A, Pyriochou A, Altaany Z, Yang G, Marazioti A, Zhou Z, Jeschke MG, Branski LK, Herndon DN, Wang R, et al. Hydrogen sulfide is an endogenous stimulator of angiogenesis. Proc Natl Acad Sci U S A. 2009; 106:21972–21977. [PubMed: 19955410]

Peng W, Robertson L, Gallinetti J, Mejia P, Vose S, Charlip A, Chu T, Mitchell JR. Surgical stress resistance induced by single amino acid deprivation requires Gcn2 in mice. Sci Transl Med. 2012; 4:118ra111.

Potente M, Ghaeni L, Baldessari D, Mostoslavsky R, Rossig L, Dequiedt F, Haendeler J, Mione M, Dejana E, Alt FW, et al. SIRT1 controls endothelial angiogenic functions during vascular growth. Genes Dev. 2007; 21:2644–2658. [PubMed: 17938244]

Potente M, Urbich C, Sasaki K, Hofmann WK, Heeschen C, Aicher A, Kollipara R, DePinho RA, Zeiher AM, Dimmeler S. Involvement of Foxo transcription factors in angiogenesis and postnatal neovascularization. J Clin Invest. 2005; 115:2382–2392. [PubMed: 16100571]

Ruckenstuhl C, Netzberger C, Entfellner I, Carmona-Gutierrez D, Kickenweiz T, Stekovic S, Gleixner C, Schmid C, Klug L, Sorgo AG, et al. Lifespan extension by methionine restriction requires autophagy-dependent vacuolar acidification. PLoS Genet. 2014; 10:e1004347. [PubMed: 24785424]

Salabei JK, Gibb AA, Hill BG. Comprehensive measurement of respiratory activity in permeabilized cells using extracellular flux analysis. Nat Protoc. 2014; 9:421–438. [PubMed: 24457333]

Schoors S, De Bock K, Cantelmo AR, Georgiadou M, Ghesquière B, Cauwenberghs S, Kuchnio A, Wong BW, Quaegebeur A, Goveia J, et al. Partial and transient reduction of glycolysis by PFKFB3 blockade reduces pathological angiogenesis. Cell Metab. 2014; 19:37–48. [PubMed: 24332967]

Sen S, Kawahara B, Gupta D, Tsai R, Khachatryan M, Roy-Chowdhuri S, Bose S, Yoon A, Faull K, Farias-Eisner R, et al. Role of cystathionine β-synthase in human breast Cancer. Free Radic Biol Med. 2015; 86:228–238. [PubMed: 26051168]

Singha S, Kim D, Moon H, Wang T, Kim KH, Shin YH, Jung J, Seo E, Lee SJ, Ahn KH. Toward a selective, sensitive, fast-responsive, and biocompatible two-photon probe for hydrogen sulfide in live cells. Anal Chem. 2015; 87:1188–1195. [PubMed: 25495776]

Smith L, Kruszyna H, Smith RP. The effect of methemoglobin on the inhibition of cytochrome c oxidase by cyanide, sulfide or azide. Biochem Pharmacol. 1977; 26:2247–2250. [PubMed: 22333]

Sonke E, Verrydt M, Postenka CO, Pardhan S, Willie CJ, Mazzola CR, Hammers MD, Pluth MD, Lobb I, Power NE, et al. Inhibition of endogenous hydrogen sulfide production in clear-cell renal cell carcinoma cell lines and xenografts restricts their growth, survival and angiogenic potential. Nitric Oxide. 2015; 49:26–39. [PubMed: 26068241]

Szabo C. Hydrogen sulphide and its therapeutic potential. Nat Rev Drug Discov. 2007; 6:917–935. [PubMed: 17948022]

Szabo C, Coletta C, Chao C, Módis K, Szczesny B, Papapetropoulos A, Hellmich MR. Tumor-derived hydrogen sulfide, produced by cystathionine-β-synthase, stimulates bioenergetics, cell proliferation, and angiogenesis in colon cancer. Proc Natl Acad Sci U S A. 2013; 110:12474–12479. [PubMed: 23836652]

Tao BB, Liu SY, Zhang CC, Fu W, Cai WJ, Wang Y, Shen Q, Wang MJ, Chen Y, Zhang LJ, et al. VEGFR2 functions as an H2S-targeting receptor protein kinase with its novel Cys1045-Cys1024 disulfide bond serving as a specific molecular switch for hydrogen sulfide actions in vascular endothelial cells. Antioxid Redox Signal. 2013; 19:448– 464. [PubMed: 23199280]

Vizan P, Sanchez-Tena S, Alcarraz-Vizan G, Soler M, Messeguer R, Pujol MD, Lee WN, Cascante M. Characterization of the metabolic changes underlying growth factor angiogenic activation: identification of new potential therapeutic targets. Carcinogenesis. 2009; 30:946–952. [PubMed: 19369582]

Wang R. Physiological implications of hydrogen sulfide: a whiff exploration that blossomed. Physiol Rev. 2012; 92:791–896. [PubMed: 22535897]

Wang Y. Molecular Links between Caloric Restriction and Sir2/SIRT1 Activation. Diabetes Metab J. 2014; 38:321–329. [PubMed: 25349818]

Wang Y, Ning Y, Alam GN, Jankowski BM, Dong Z, Nör JE, Polverini PJ. Amino acid deprivation promotes tumor angiogenesis through the GCN2/ATF4 pathway. Neoplasia. 2013; 15:989–997. [PubMed: 23908598]

Wek SA, Zhu S, Wek RC. The histidyl-tRNA synthetase-related sequence in the eIF-2 alpha protein kinase GCN2 interacts with tRNA and is required for activation in response to starvation for different amino acids. Mol Cell Biol. 1995; 15:4497– 4506. [PubMed: 7623840]

Whiteman M, Armstrong JS, Chu SH, Jia-Ling S, Wong BS, Cheung NS, Halliwell B, Moore PK. The novel neuromodulator hydrogen sulfide: an endogenous peroxynitrite ‘scavenger’? J Neurochem. 2004; 90:765–768. [PubMed: 15255956]

Whiteman M, Cheung NS, Zhu YZ, Chu SH, Siau JL, Wong BS, Armstrong JS, Moore PK. Hydrogen sulphide: a novel inhibitor of hypochlorous acid-mediated oxidative damage in the brain? Biochem Biophys Res Commun. 2005; 326:794–798. [PubMed: 15607739]

Yadav V, Gao XH, Willard B, Hatzoglou M, Banerjee R, Kabil O. Hydrogen sulfide modulates eukaryotic translation initiation factor 2alpha (eIF2alpha) phosphorylation status in the integrated stress-response pathway. J Biol Chem. 2017; 292:13143–13153. [PubMed: 28637872]

Yang G, Wu L, Jiang B, Yang W, Qi J, Cao K, Meng Q, Mustafa AK, Mu W, Zhang S, et al. H2S as a physiologic vasorelaxant: hypertension in mice with deletion of cystathionine gamma-lyase. Science. 2008; 322:587–590. [PubMed: 18948540]

Yong R, Searcy DG. Sulfide oxidation coupled to ATP synthesis in chicken liver mitochondria. Comp Biochem Physiol B Biochem Mol Biol. 2001; 129:129–137. [PubMed: 11337256]

Highlights

- Sulfur amino acid (SAA) restriction triggers angiogenesis independent of hypoxia or HIF1α
- GCN2/ATF4 pathway regulates VEGF and CGL expression upon SAA restriction in ECs
- CGL is required for skeletal muscle angiogenesis activated by diet or exercise
- H_2S triggers glucose uptake, glycolysis and PPP concomitant with OXPHOS inhibition in ECs

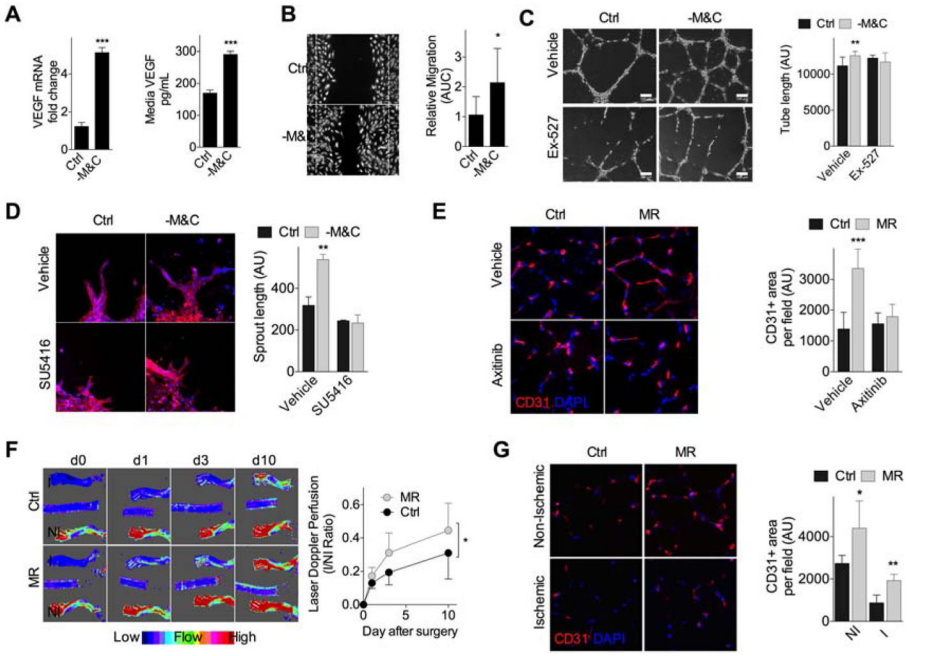

Figure 1. SAA restriction induces endothelial VEGF expression *in vitro* and functional angiogenesis *in vivo*

(**A**) VEGF mRNA levels (left, n=4 experiments/group) and secreted protein concentration in the media (right, n=6 experiments/group) of HUVEC cultured in control (Ctrl) or SAA deficient (- M&C) media for 16hr; error bars indicate SEM. **(B)** Migration assay: Representative migration across a scratch (left, 10X mag at t=20hr; dotted lines indicate boundary of the scratch at t= 0hr) and area under the curve (AUC, right, n=7–10 data points/condition, with each data point representing the mean of multiple measures within a single well in a representative experiment) from HUVEC cultured in the indicated media. (**C**) Tube formation assay: Representative capillary-like structures (left, 40X mag) and quantification of tube length/field in arbitrary units (AU, right; n=8–10 data points/condition) in HUVEC incubated in the indicated media +/−SIRT1 inhibitor Ex-527 for 18hr. (**D**) Spheroid assay: Representative images (left, 40X mag) and quantification (right, in triplicate) of sprouting HUVEC spheroids in the indicated media +/− VEGFR2 inhibitor SU5416 for 24hr; blue, DNA (DAPI); red, F-actin (phalloidin). (**E**) Representative transverse sections (left, 40X mag) and quantification (right) of gastrocnemius muscle stained for endothelial marker CD31 in mice fed 2wk on Ctrl or MR diet +/−VEGFR2 inhibitor axitinib; n=6–8 mice/group. (**F**) Longitudinal Doppler imaging of blood flow in WT mice preconditioned 1mo on Ctrl or MR diet prior to femoral artery ligation (I, ischemic; NI, non-ischemic). Left: representative infrared images on the indicated day after ligation. Right: quantification of blood flow recovery with individual animal AUCs used for statistical comparison; n=7–8 mice/group. (**G**) Representative transverse sections (left, 40X mag) and quantification (right) of CD31-stained gastroc 10d after ligation from (**F**); n=4 mice/group. Error bars indicate SD unless otherwise noted; asterisks indicate the significance of the difference by Student's T test or 1-way ANOVA with Sidak's MCT between diets *in vivo* or SAA deprivation *in vitro*; **P*<0.05, ***P*<0.01, ****P*<0.001. See also Fig. S1.

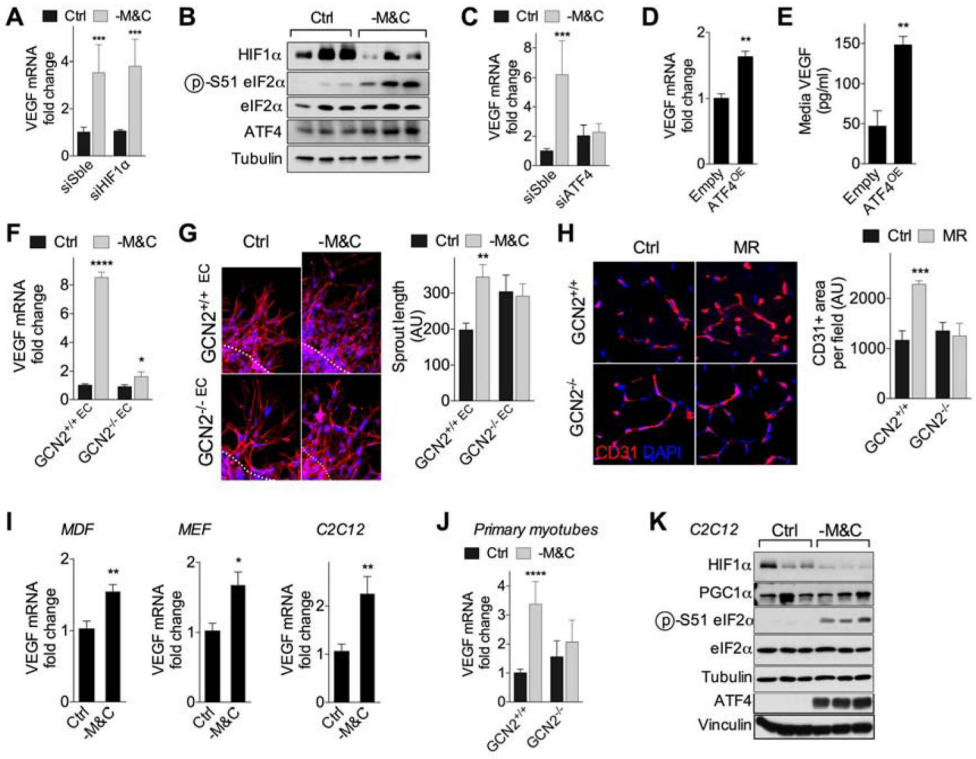

Figure 2. GCN2-dependent, hypoxia-independent regulation of VEGF and angiogenesis upon SAA restriction

(**A)** Relative VEGF mRNA expression in HUVEC 2d after transfection with HIF1α siRNA or control scrambled (Sble) siRNA and cultured in control (Ctrl) or SAA deficient (-M&C) media for 16hr; n=5 experiments/group; error bars indicate SEM. (**B**) Immunoblots of HIF1α, eIF2α (p- Ser51, total) and ATF4 in HUVEC cultured as indicated for 16hr. (**C**) Relative VEGF mRNA expression in HUVEC 2d after transfection with ATF4 or Sble siRNA and cultured as indicated for 16hr; n=4 experiments/group; SEM. (**D, E**) Relative HUVEC VEGF mRNA expression (**D,** n=3 experiments/group; SEM) and secreted VEGF protein concentration in media (**E,** n=3–6 experiments/group; SEM) 2d after transfection with ATF4 overexpression ($ATF4^{OE}$) or control construct (Empty). (**F, G**) VEGF mRNA expression (**F**) and spheroid formation (**G**) in WT and GCN2KO primary mouse EC from n=3 mice/genotype cultured as indicated for 16hr. For sprouting assay (**G**), representative images (left, 40X mag) and quantification (right) of WT and GCN2KO EC spheroids cultured in the indicated media for 24hr; blue, DNA (DAPI); red, F-actin (phalloidin). (**H**) Representative transverse sections (left, 40X mag) and quantification (right) of CD31-stained gastroc in WT or GCN2KO mice fed for 2–4wk on Ctrl or MR diets; n=5–6 mice/group. (**I**) VEGF mRNA in MDF, MEF or C2C12 myotubes cultured as indicated for 16hr; n=4–6 experiments/group; SEM. (**J**) VEGF mRNA expression in WT and GCN2KO primary mouse skeletal myotubes (n=5 mice/genotype tested at 2 different passages) cultured as indicated for 16hr. (**K**) Immunoblots of HIF1α, PGC1α, eIF2α (p-Ser51, total) and ATF4 in C2C12 myotubes cultured as indicated for 16hr. Error bars indicate SD unless otherwise noted; asterisks indicate the significance of the difference by Student's T test or 1-

way ANOVA with Sidak's MCT between diets *in vivo* or SAA deprivation *in vitro*; *$P<0.05$, **$P<0.01$, ***$P<0.001$. See also Fig. S2.

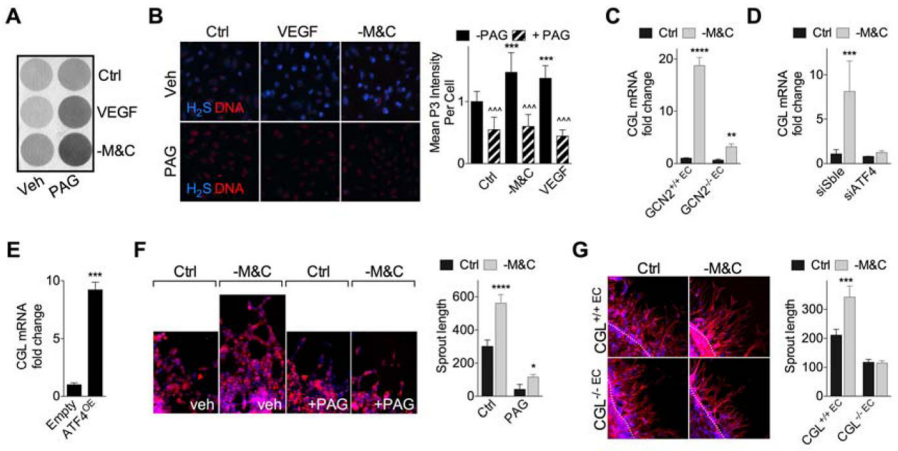

Figure 3. VEGF signalling and AASR converge on endothelial H_2S production by CGL

(**A**) Representative H_2S production capacity as indicated by black lead sulfide formation from HUVEC cultured in media +/−M&C or VEGF (50ng/mL) in the presence or absence of the CGL inhibitor PAG (100μM) as indicated for 16hr. (**B**) Representative (left) endogenous H_2S levels (blue, H_2S (P3 fluorescence); red, DNA (DRAQ5)) and quantification of P3 intensity (right) in HUVEC upon VEGF or -M&C treatment; n=4 wells/treatment with 4–6 images/well; 1-way ANOVA with Sidak's MCT vs. Control (asterisks) or +/−PAG within treatment (carets). (**C**) CGL mRNA expression in WT and GCN2KO primary mouse EC cultured from n=3 mice/genotype in control (Ctrl) or -M&C media for 16hr. (**D**) CGL mRNA expression in HUVEC 2d after transfection with ATF4 or control scrambled (Sble) siRNA and cultured in the indicated media for 16hr; n=4 experiments/group; SEM. (**E**) CGL mRNA expression in HUVEC 2d after transfection with ATF4 overexpression or control (empty) plasmid; n=3 experiments/group; SEM. (**F, G**) Representative images (left, 40X mag) and quantification (right, in triplicate) of spheroids cultured from (**F**) HUVEC +/−M&C for 24hr in the presence of vehicle (Veh) or PAG, and (**G**) WT or CGLKO primary EC sprouts in control or -M&C media for 24hr; blue, DNA (DAPI); red, F-actin (phalloidin). Unless otherwise indicated, error bars indicate SD, and asterisks indicate the significance of the difference between diets *in vivo* or SAA levels *in vitro* by Student's T test or 1-way ANOVA with Sidak's MCT; **P*<0.05, ***P*<0.01, ***/^^^*P*<0.001. See also Fig. S3.

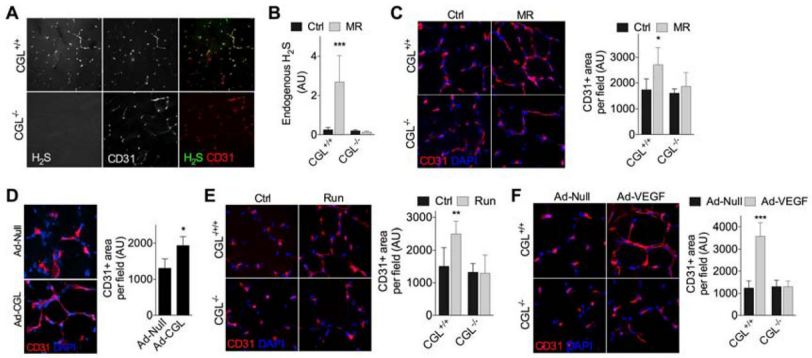

Figure 4. CGL required for angiogenesis *in vivo*

(**A**) Representative transverse sections (20X mag) of gastrocnemius muscle from WT and CGLKO mice stained for CD31 and endogenous H_2S. (**B**) Quantification of endogenous H_2S in $CD31^+$ EC in the gastrocnemius muscle of WT and CGLKO mice fed for 2wk on Ctrl or MR diets as indicated; n=4–5 mice/group, with quantification of 3–10 images/mouse. (**C**) Representative transverse sections (left, 40X mag) and quantification (right) of CD31-stained gastroc from WT and CGLKO mice fed for 2wk on Ctrl or MR diets as indicated; n=4 mice/group. (**D**) Representative transverse sections of CD31-stained gastroc (left, 40X mag) and quantification (right) 2wk after Ad-Null or Ad-CGL injections; n=3–4 mice/group; Student's T test. (**E**) Representative transverse sections (left, 40X mag) and quantification (right) of CD31-stained gastroc from WT and CGLKO mice subjected to low intensity running (exercised) vs. control (sedentary) for 1mo; n=4–5 mice/group. (**F**) Representative transverse sections of CD31-stained gastroc (left, 40X mag) and quantification (right) from WT and CGLKO mice 6d after the final intramuscular injection of control (Ad-Null) or $VEGF_{165}$ -expressing (Ad-VEGF) adenovirus; n=4 mice/group. Error bars indicate SD; asterisks indicate the significance of the difference between diets or treatments within genotype by 1-way ANOVA with Sidak's MCT unless otherwise noted; *P<0.05, **P<0.01, ***P<0.001. See also Fig. S4.

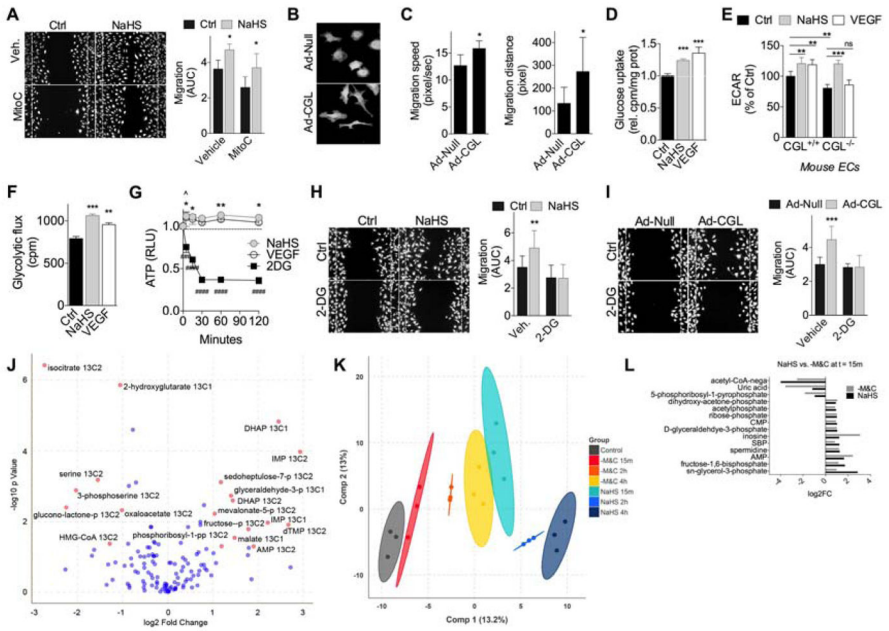

Figure 5. H_2S promotes glucose uptake and ATP generation by glycolysis for EC migration

(**A**) Representative migration across scratch (left, 10X mag) and quantification (right) of HUVEC +/−100μM NaHS in the presence of vehicle or mitomycin C (MitoC, 1μg/mL) to inhibit proliferation; n=12 wells each from cells at 2 different passages; 1-way ANOVA with Sidak's MCT between control and NaHS within vehicle or MitoC treatment group. (**B, C**) Representative images (**B**) and quantification (**C**) of migration speed (left, n=5–7 cells/condition) and distance (right, n=5–7 cells/condition in x and y directions) from time-lapse video imaging of GFP+ HUVEC infected with control (Ad-Null) or CGL adenovirus (Ad-CGL) as indicated; Student's T test. (**D**) Relative glucose uptake in HUVEC pretreated with NaHS or 50ng/mL VEGF for 1hr; n=3–6 experiments/group; 1-way ANOVA with Dunnett's MCT. (**E**) Extracellular acidification rate (ECAR) in WT and CGLKO primary mouse EC pretreated for 1hr with VEGF or NaHS; 10 technical replicates from EC pooled from 6 mice/genotype; 1-way ANOVA with Sidak's MCT as indicated. (**F**) Glycolytic flux in HUVEC pretreated for 3hr with NaHS or VEGF; 1-way ANOVA with Dunnett's MCT. Representative experiment of 6 with n=3/group; 1-way ANOVA with Sidak's MCT. (**G**) Time dependent ATP production in HUVEC pretreated with NaHS or 1mM 2DG at t=0; n=4 experiments each for NaHS and VEGF and 2 for 2DG; error bars indicate SEM; 2-way ANOVA with Dunnett's MCT relative to t=0 (asterisk, NaHS; caret, VEGF; pound sign, 2DG). (**H, I**) Representative migration (left, 10X mag) and quantification (right, AUC) of HUVEC treated +/−NaHS (**H,** n=11 technical replicates/condition) or infected with a control (Ad-Null) or CGL adenovirus (Ad-CGL) at a multiplicity of infection of 50 (**I,** n=5–6 technical replicates/condition), in the presence of vehicle or 2DG; 1-way ANOVA with Sidak's MCT between control and NaHS within 2DG or vehicle treatment group. (**J**) Log2 fold change of C13- labelled metabolites in HUVEC measured by mass spectrometry after 1hr of NaHS pretreatment compared to control; red dots, metabolites with FDR adjusted P<0.05 and absolute value of log2 fold change>1.2; blue dots, metabolites with FDR adjusted P>0.05 and/or absolute value of log2 fold change<1.2. (**K**) Plot of the first two

components of orthogonal partial least squares discriminant analysis on unlabeled metabolite levels in HUVEC after 15min, 2hr or 4hr treatment with NaHS or -M&C. Ellipses represent 99% confidence bound for treatment groups. (**L**) Average metabolite log2 fold changes after 15min of NaHS or -M&C. All metabolites that significantly (P<0.05) changed in the same direction in both treatment groups are shown. Error bars indicate SD unless otherwise indicated; */^P<0.05, ** P<0.01, ***/### P<0.001, #### P<0.0001. See also Fig. S5.

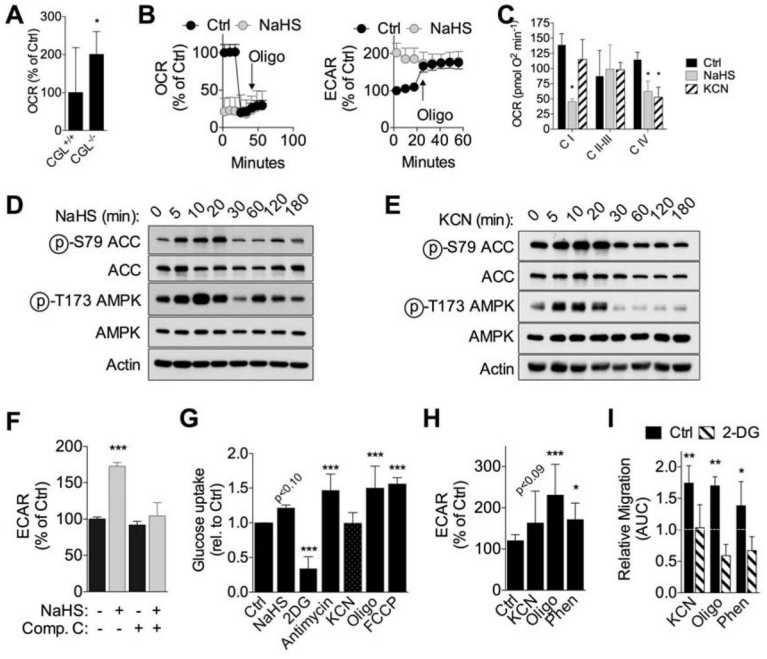

Figure 6. H_2S shifts oxidative/glycolytic balance concomitant with inhibition of mitochondrial OXPHOS

(**A**) Basal oxygen consumption rate (OCR) in WT and CGLKO primary mouse EC; n=10 technical replicates from EC pooled from 6 mice/genotype; Student's T test. (**B**) OCR (left) and extracellular acidification rate (ECAR, right) in HUVEC pretreated for 2hr with 100μM NaHS followed by oligomycin (oligo, 2.5μM) injection at the indicated time; representative experiment with n=10 technical replicates/treatment. (**C**) Mitochondrial complex activity in permeabilized HUVEC pretreated for 1hr with NaHS or 10μM KCN ; representative experiment with n=6 technical replicates; 1-way ANOVA with Sidak's MCT within complex activity group. (**D, E**) Immunoblots of ACC (pSer79, total) and AMPK (Thr172, total) in HUVEC treated with NaHS (**D**) or KCN (**E**) for the indicated time. (**F**) ECAR in HUVEC pretreated for 1hr with NaHS +/−10μM Compound C (Comp C, an AMPK inhibitor) as indicated; n=10 technical replicates from EC pooled from 6 mice/genotype; 1-way ANOVA with Sidak's MCT between NaHS treatment within Comp C treatment group. (**G**) Relative glucose uptake in HUVEC pretreated with the indicated agent for 1–3hr; n=2–8 experiments/group; error bars indicate SEM; 1-way ANOVA with Dunnett's MCT. (**H**) ECAR in HUVEC pretreated for 2hr with KCN, 2μM oligo or phenformin (Phen, 500μM) expressed as a percent of control over time after addition of 10mM glucose; n=12–19 technical replicates; 1-way ANOVA with Dunnett's multiple comparison test. (**I**) Migration across scratch expressed as fold change relative to control in HUVEC treated with oligomycin (2μM), phenformin or KCN +/−2DG (1mM) as indicated; n=5–12 AUC values/group each from cells at different passages; 1-way ANOVA with Sidak's MCT vs. control without 2DG treatment. Error bars indicate SD unless otherwise noted; *P<0.05, **P<0.01, ***P<0.001. See also Fig. S6.

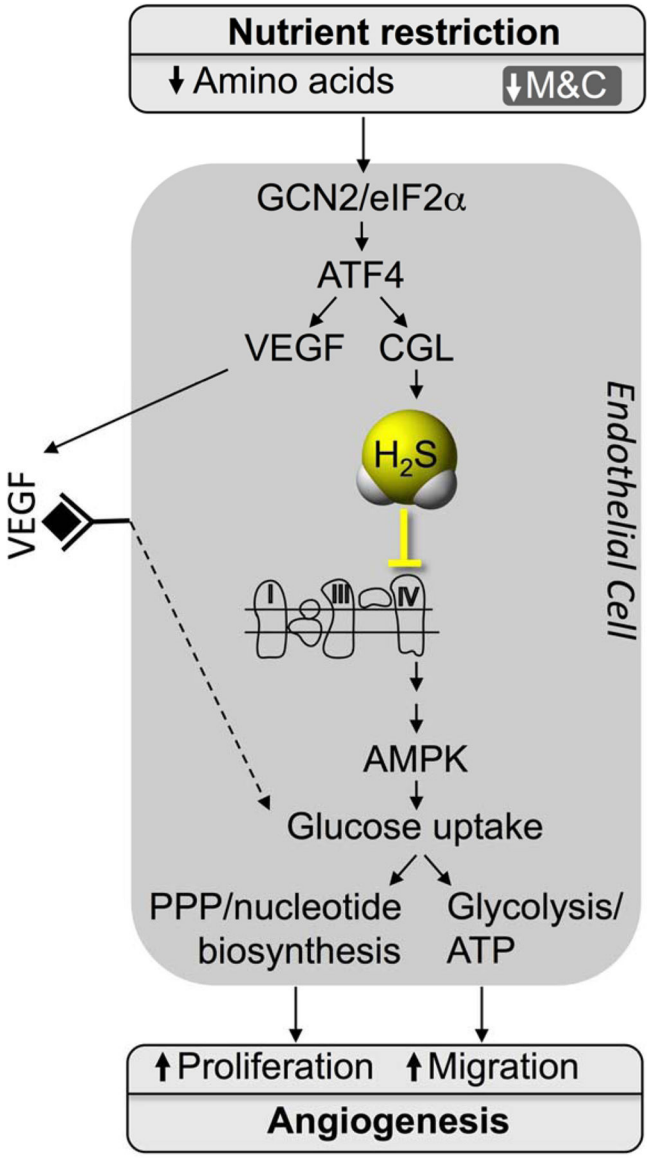

Figure 7. Model for regulation of angiogenesis by AA restriction

GCN2/ATF4 pathway activation in EC by AA restriction induces VEGF expression as well as CGL-mediated H_2S production with effects on glucose uptake and utilization via glycolysis and PPP required for EC migration and proliferation.

KEY RESOURCES TABLE

REAGENT or RESOURCE	SOURCE	IDENTIFIER
Antibodies		
Anti-CGL (Anti-Cystathionase)	Abcam	Cat# Ab151769
Anti-CBS	Abcam	Cat# Ab135626
Anti-3MST (Anti-MPST)	Sigma	Cat# HPA001240
Anti-ATF4 (Anti-CREB-2)	Santa Cruz	Cat# Sc-200
Anti-beta Tubulin	Cell Signaling	Cat# 2128
Anti-Actin	Cell Signaling	Cat# 4970
HRP conjugated anti-rabbit	Dako	Cat# P044801-2
Anti-CD31	BD Bioscience	Cat# 557355
Anti-HIF1a	Cayman Chemical	Cat# 10006421
Anti-p-eIF2α Ser51	Cell Signaling	Cat# 9712S
Anti-total eIF2α	Cell Signaling	Cat# 9722S
Anti-Tubulin	Cell Signaling	Cat# 2146S
Anti-CD31-APC	Biolegend	Cat# 102410
Alexa Fluor 555 phalloidin	ThermoFisher	Cat# A34055
Bacterial and Virus Strains		
Ad-CMV-CGL (Ad-mCTH)	Vector Biolabs	Cat# ADV-256305
Ad-CMV-Null	Vector Biolabs	Cat# 1300
Ad-h-VEGFA165	Vector Biolabs	Cat# ADV-227457
Ad-m-ATF4-shRNA	Vector Biolabs	Cat# shADV-253208
Ad-GFP	Vector Biolabs	Cat# 1060
Biological Samples		
Livers (frozen) taken from experimental mouse strains listed in the Experimental Models: Organisms/Strains section	See Experimental Models: Organisms/ Strains section	See Experimental Models: Organisms/Strains section
Serum/Plasma (frozen) taken from experimental mouse strains listed in the Experimental Models: Organisms/Strains section	See Experimental Models: Organisms/ Strains section	See Experimental Models: Organisms/Strains section
Skeletal muscle (frozen) taken from experimental mouse strains listed in the Experimental Models: Organisms/Strains section	See Experimental Models: Organisms/ Strains section	See Experimental Models: Organisms/Strains section
Chemicals, Peptides, and Recombinant Proteins		
NaHS	Sigma	Cat# 161527
GYY4137	Sigma	Cat# SML0100
DL-Propargylglycine	Sigma	Cat# P7888
Passive Lysis Buffer (5x)	Promega	Cat# E1941
PLP (Pyridoxal 5′-phosphate)	Sigma	Cat# P9255
L-cysteine	Sigma	Cat# C7352
Lead (II) acetate trihydrate	Sigma	Cat# 316512

REAGENT or RESOURCE	SOURCE	IDENTIFIER
P3 H2S Detection Probe	From the lab of Prof. K.H. Ahn	Singha et al., 2015
SU5146	Tocris	Cat. No. 3037
Ex-527	Cayman Chemical	Cat# 10009798
VECTASHIELD Antifade Mounting Medium with DAPI	Vector laboratories	Cat# H-1200
Potassium Cyanide	Sigma	Cat# 11813
Phenformin	Sigma	Cat# P7045
2-Deoxy-D-Gucose	Sigma	Cat# D8375
Oligomycin A	Sigma	Cat# 75351
FCCP (Carbonyl cyanide 4-(trifluoromethoxy)phenylhydrazone)	Sigma	Cat# C2920
Antimycin A	Sigma	Cat# A8674
MitomycinC	Sigma	Cat# M4287-2MG
Compound C (Dorsomorphin)	Abcam	Cat# Ab120843
Axitinib	Selleckchem	Cat# S1005
L-NAME (hydrochloride)	Cayman Chemical	Cat# 80210
Recombinant human VEGF165	Peprotech	Cat# 100-20
Recombinant murine VEGF165	Peprotech	Cat# 450-32
Propidium Iodine	ThermoFisher Scientific	Cat# P3566
Annexin V	ThermoFisher Scientific	Cat# A13201
Critical Commercial Assays		
Mouse VEGF ELISA	Peprotech	Cat# 900-K99
Mouse VEGF Quantikine ELISA kit	R&D Systems	Cat# MMV00
Human VEGF Quantikine ELISA kit	R&D Systems	Cat# DVE00
Deposited Data		
Experimental Models: Cell Lines		
Primary mouse endothelial cells prepared from C57BL/6, CGL KO, GCN2 KO and SIRT1 inducible KO mice (freshly isolated in the lab of Dr. James Mitchell or Dr. David Sinclair for each experiment)	Jackson Laboratories and laboratory of Dr. James R. Mitchell	Cat# 000664; this paper; Das et al. in this issue
Primary mouse myotubes from GCN2 WT and KO mice	From the laboratory of Dr. James R. Mitchell	This paper
Primary CGL WT and KO mouse tail dermal fibroblasts	From the laboratory of Dr. James R. Mitchell	This paper
Primary mouse hepatocytes from WT mice	From the laboratory of Dr. James R. Mitchell	This paper
Immortalized MEF	From the laboratory of Dr. James R. Mitchell	This paper
HUVEC	Lonza	Cat# CC-2519
C2C12	ATCC	Cat# CRL-1772
Experimental Models: Organisms/Strains		

REAGENT or RESOURCE	SOURCE	IDENTIFIER
C57BL/6 male and female Mice	Jackson Laboratories	Cat# 000664
WT and KO CGL male and female mice on mixed 129/C57BL/6 background	Strain originally from Dr. Rui Wang and bred in the lab of Dr. James R. Mitchell	Yang et al., 2008; Hine et al., 2015
GCN2 WT and KO male and female mice	Strain originally from Dr. David Ron and bred in the lab of Dr. James R. Mitchell	Munn et al., 2005; Peng et al., 2012
Oligonucleotides		
si-Scramble (Selective negative control No.1 siRNA)	ThermoFisher Scientific	Cat# 4390843
Mouse si-PGC1a (PPARGC1A)	ThermoFisher Scientific	Cat# n253420
Mouse si-HIF1a	ThermoFisher Scientific	Cat# s67530
Human si-ATF4	ThermoFisher Scientific	Cat# s1704
Human si-PGC1alpha (PPARGC1A)	ThermoFisher Scientific	Cat# s21394
Human si-HIF1a (HIFA)	ThermoFisher Scientific	Cat# s6539
Human si-eNOS (NOS3)	ThermoFisher Scientific	Cat# s9623
human ACTIN/ACTB F: GTTGTCGACGACGAGCG R: GCACAGAGCCTCGCCTT	N/A	N/A
human ASNS F: GCGGAGTGCTTCAATGTAAC R: CCAATAAGAAAGTGTTCCTGGG	N/A	N/A
human ATF4 F: CTATACCCAACAGGGCATCC R: GTCCCTCCAACAACAGCAAG	N/A	N/A
For a full list of all primers used, please see Table S1		
Recombinant DNA		
prK-ATF4 overexpression plasmid	Addgene	26114
Software and Algorithms		
ImageJ	National Institutes of Health	https://imagej.nih.gov/ij/download.html
GraphPad Prism	GraphPad	Version 7.0
FlowJo	FlowJo LLC	https://www.flowjo.com/solutions/flowjo
Fiji software	GPL v2, Fiji	http://fiji.sc/Fiji
Matlab R2017A	MathWorks	https://www.mathworks.com/programs/trials/trial_request.html?prodcode=ML
Other		